

27. SONIC AND ULTRASONIC LOGGING OF HOLE 504B AND ITS IMPLICATIONS FOR THE STRUCTURE, POROSITY, AND STRESS REGIME OF THE UPPER 1 KM OF THE OCEANIC CRUST¹

Robin L. Newmark and Roger N. Anderson, Lamont-Doherty Geological Observatory

Daniel Moos, Stanford University and United States Geological Survey

and

Mark D. Zoback, United States Geological Survey²

ABSTRACT

The layered structure of the oceanic crust is characterized by changes in geophysical gradients rather than by discrete layer boundaries. Correlation of geophysical logs and cores recovered from DSDP Hole 504B provides some insight into the physical properties that control these gradient changes. Borehole televiewer logging in Hole 504B provides the deepest continuous image of well-bore reflectivity into the oceanic crust, revealing detailed structures not apparent otherwise, because of the low percentage of core recovery. Physical characteristics of the crustal Layers 2A, 2B, and 2C, such as the detailed sonic velocity and lithostratigraphic structure, are obtained through analysis of the sonic, borehole televiewer, and electrical resistivity logs. A prediction of bulk hydrated mineral content, consistent with comparison to the recovered material, suggests a change in the nature of the alteration with depth. Data from the sonic, borehole televiewer, electrical resistivity, and other porosity-sensitive logs are used to calculate the variation of porosity in the crustal Layers 2A, 2B, and 2C. Several of the well logs that are sensitive to the presence of fractures and open porosity in the formation indicate many zones of intense fracturing. Interpretation of these observations indicates that there may be a fundamental pattern of cooling-induced structure in the oceanic crust.

INTRODUCTION

Most of our understanding of the structure of the oceanic crust is derived from extrapolation of seabed geology combined with remote geophysical studies. The layered structure of the oceanic crust has been defined by changes in the rate of increase of seismic velocities with depth (Helmberger and Morris, 1970; Orcutt et al., 1976; Spudich and Orcutt, 1980). Comparison with ophiolites has provided a model to describe the structural, lithologic, and petrologic conditions responsible for the layered structure (Dietz, 1963; Hess, 1962; Fox et al., 1973), which has been shown to exhibit variations with both depth and age (Houtz and Ewing, 1976).

Houtz and Ewing (1976) described a horizontal variability in seismic Layer 2. The thickness of seismic Layer 2A decreases with increasing age, and the layer effectively "disappears" on the flanks of the mid-ocean ridges. They suggested that the increase in the velocity of seismic Layer 2A with age is a function of either unspecified diagenetic processes and/or off-ridge-axis volcanism. Other workers (Schreiber and Fox, 1976, 1977; Hyndman and Drury, 1976) have suggested that the dominant control on the seismic character of this zone is the frequency of cracks and void space within the upper several hundred meters of oceanic crust. Combining the

results of Houtz and Ewing (1976) with the observation that cracks in weathered basalts recovered by the Deep Sea Drilling Project were often filled with low-temperature minerals led Schreiber and Fox (1976, 1977) to suggest that over time the percentage of water-filled cracks in Layer 2A changes. The igneous mineral phases exposed along water-filled cracks react with water to produce low-temperature alteration products, which are less dense than the primary phases and therefore will expand to fill and eventually seal the cracks. Consequently, the shallow crust will seal with time, and the bulk seismic velocity will increase. It is of great interest to establish both the extent and nature of alteration and porosity in the upper oceanic crust.

The drilling of DSDP Hole 504B during Leg 83 beyond 1 km depth into the crust has provided us with the first opportunity to compare *in situ* geophysical measurements and recovered core with the ophiolite model through seismic Layers 1, 2A, 2B, and 2C. During previous legs the sediments of Layer 1, the basaltic pillows and flows of Layer 2A, and some of the metamorphosed pillows and flows of Layer 2B were cored and described (CRRUST, 1982; Cann, Langseth, Honnorez, Von Herzen, White, et al., 1983). Leg 83 completed drilling through the transition from metamorphosed pillows and flows of Layer 2B to the dikes of Layer 2C and over 350 m into the sheeted dikes of Layer 2C. In addition, an integrated suite of downhole geophysical experiments was conducted to investigate the changes in the physical properties as a result of the layered structure. These include a complete set of downhole geophysical logs, including multichannel sonic velocity logging (Anderson, O'Malley, and Newmark, this volume), and permeability and pore-pressure measurements (Anderson, Zoback, et al.,

¹ Anderson, R. N., Honnorez, J., Becker, K., et al., *Init. Repts. DSDP*, 83: Washington (U.S. Govt. Printing Office).

² Addresses: (Newmark) Borehole Research Group, Lamont-Doherty Geological Observatory, Columbia University, Palisades, NY 10964, and Department of Geological Sciences, Columbia University; (Anderson) Borehole Research Group, Lamont-Doherty Geological Observatory, Columbia University, Palisades, NY 10964; (Moos; present address) Borehole Research Group, Lamont-Doherty Geological Observatory, Columbia University, Palisades, NY 10964; (Zoback) Branch of Tectonophysics, United States Geological Survey, Menlo Park, CA 94025.

this volume). In this chapter, we report results of ultrasonic borehole televiewer imaging conducted in this hole to determine the lithostratigraphy and fracture distribution in the oceanic crust. Correlation of these images with conventional geophysical logs and recovered cores has provided us with insight into the relationships among these physical properties and into their implications for the evolution of the oceanic crust.

SONIC LOGGING

Sonic logging during Leg 83 was accomplished using the Schlumberger two-transmitter, two-receiver sonic sonde, run in several modes. (Complete descriptions of the logging runs and tool can be found in the Hole 504B summary chapter, this volume; Anderson, O'Malley, and Newmark, this volume.) First, a traditional P-wave first arrival log was run. Next, full waveform digitization of all four channels was recorded. Finally, an *in situ* S-wave log was recorded by setting a moving-gate window to exclude the P-wave arrival and record the large-amplitude S-wave arrival. The shear velocities obtained during this last sonic logging run were later verified in the lower part of the hole by comparison with shear wave velocities obtained by shore-based direct calculation from the full waveforms.

Figure 1 shows the downhole sonic velocities obtained in the upper 1 km of oceanic crust at Hole 504B. On the left of the figure is a generalized section indicating the dominant lithologic units with depth. In the center are 10-m running averages of the downhole P and S velocities from the first and last logging runs. (The nonaveraged P and S velocities can be seen in Fig. 2.) On the right is a simplified velocity model based on the sonic logs where the sediment layer is divided into three layers and the basalt section is represented by 100 layers 10 m thick.

The uppermost 100 m of basement is an aquifer of rubbly pillow basalts, breccias, and a few massive flows (CRRUST, 1982; Cann, Langseth, Honnorez, Von Herzen, White, et al., 1983). Here we see variable, but generally low P and S velocities, which is more apparent in the nonaveraged data shown in Figure 2. The average P-wave velocity in this upper 100 m is 3.7 ± 0.8 km/s and the average S-wave velocity in this interval is 2.1 ± 0.7 km/s. These average velocities fall within the general bounds for Layer 2A velocities stated by Fox and Stroup (1981): 2.8–4.5 km/s for P-waves and 2.2–2.6 km/s for S-waves. Although the upper 200 m is characterized by steep velocity gradients, the greatest variability and steepest gradients appear in the upper 100 m, which we interpret to be seismic Layer 2A.

The next 550 m is composed of pillow basalts, flows, and breccias, and contains an abundance of hydrated minerals and alteration products. This section is characterized by moderate velocity gradients in both P and S. The average P-wave velocity is 4.8 ± 0.8 km/s and the average S-wave velocity is 2.8 ± 0.3 km/s. These values fall well within the range for Layer 2B velocities of 4.5–5.7 km/s for P-waves and 2.6–3.5 km/s for S-waves (Fox and Stroup, 1981).

The lower 350 m of the hole penetrated sheeted dikes. This section of the hole shows moderately increasing P-wave velocities and nearly constant S-wave velocities. The average P-wave velocity is 5.6 ± 0.3 km/s, and the average S-wave velocity is 3.3 ± 0.2 km/s. These values are low but near the range for Layer 2C velocities of 5.7–6.7 km/s (Fox and Stroup, 1981). We interpret this section to be the upper part of seismic Layer 2C. We assume that the P and S velocities will continue to increase with depth through this section; thus the average overall layer velocity will be higher.

These divisions of the drilled section into Layers 2A, 2B, and 2C agree well with the striking stratification of porosity derived from the large-scale resistivity experiment by Becker et al. (1982, 1983) and Becker (this volume) as well as other changes in physical properties described by Anderson et al. (1982).

Superimposed on our velocity model in Figure 1 can be seen the best-fit velocity-depth model solution for Layer 2B from the borehole seismic experiment run in Hole 504B by Stephen and Harding (1983). The best-fit velocity-depth solution required a two-layer model including Layers 2B and 2C. The borehole seismic experiment showed no evidence for Layer 2A, but a 100-m-thick layer may be beyond the resolution of both that experiment and conventional refraction techniques (Houtz and Ewing, 1976). Stephen's (1983) best-fit model shows an integration or average of the more detailed structure. There are three major low-velocity zones in the profile and several smaller ones. It seems as though the borehole seismic experiment responds to the high-velocity cap at the top of the crustal section and does not "see" the low-velocity zone directly below.

BOREHOLE TELEVIEWER

A major factor limiting interpretation of the lithostratigraphy of the oceanic crust using deep-sea drilling results from the *Glomar Challenger* is the low percentage of core recovery. The ultrasonic borehole televiewer (BHTV) is the only wireline logging tool capable of providing a continuous image of the borehole wall. Borehole televiewer images can provide the essential structural information necessary to correlate and interpret the various geophysical logs with respect to the recovered core. This is particularly important in instances of low core recovery, such as on Leg 83 where the average recovery was 20% overall, and less than 15% in the dikes. The BHTV records from Hole 504B can be found in Appendix A.

A description of the tool operation and the two logging runs during Leg 83 can be found in the chapter on *in situ* stress measurements (Newmark, Zoback, and Anderson, this volume) and in the Hole 504B Site chapter, this volume. There is also a general description of techniques of interpretation of the BHTV records in the Hole 504B site chapter and a lithostratigraphic correlation that provides an accurate representation of the *in situ* locations of the recovered material in the section.

The borehole televiewer contains a rotating piezoelectric transducer which emits and receives an ultra-

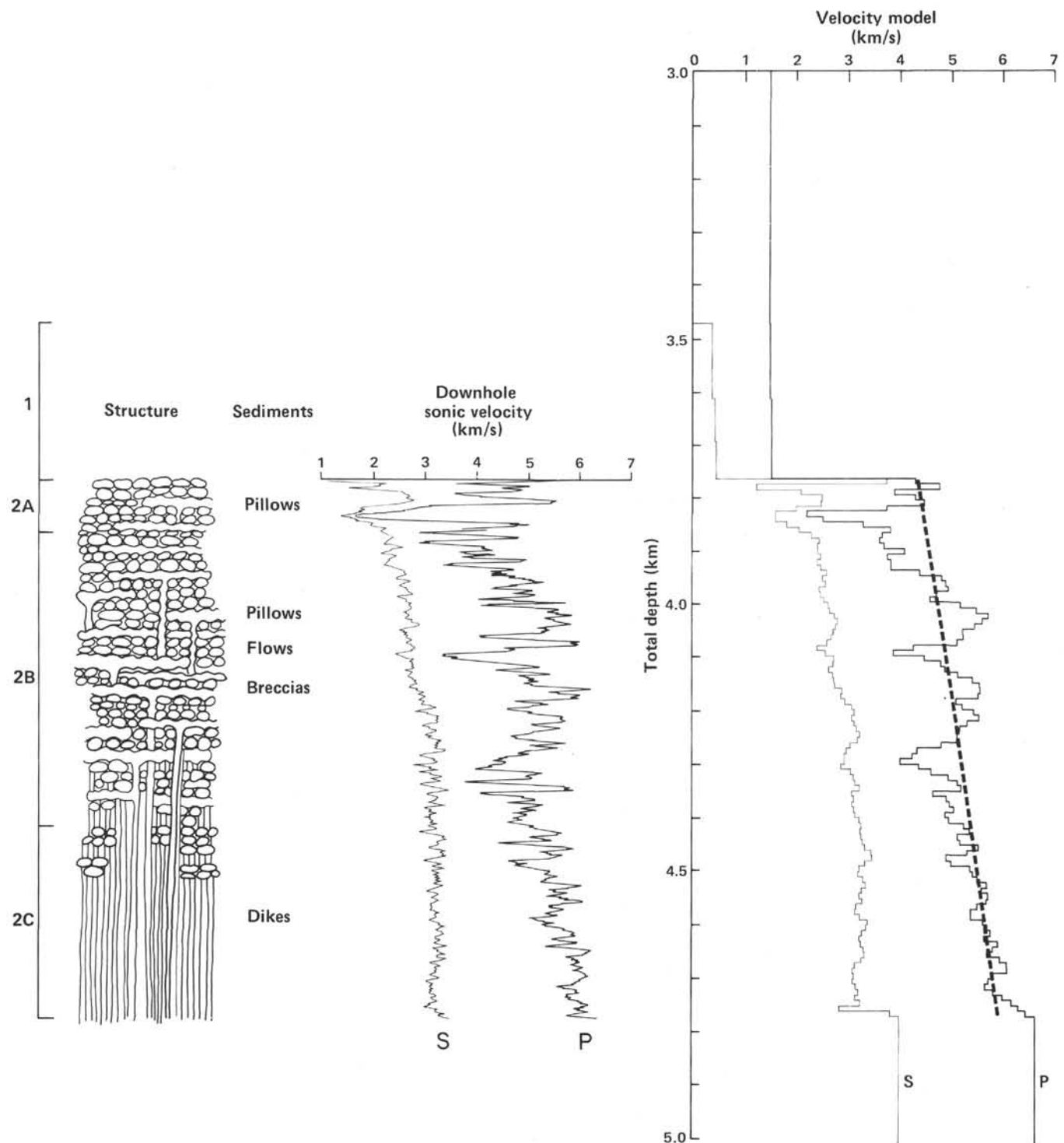


Figure 1. Downhole sonic velocities in the upper 1 km of basement in DSDP Hole 504B. On left is a schematic section indicating dominant lithologic units with depth. In the center are 10-m running averages of the downhole P and S velocities. On the right is a simplified velocity model where the sediment column is divided into three layers and the basement is divided into 100 10-m-thick layers. Dashed line is Stephen's (1983) best-fit velocity-depth model Solution for Layer 2B.

high-frequency (1.3 MHz) acoustic pulse in a 3° beam, 1800 times a second (see Fig. 3). Zemanek et al. (1970) describe the operation of the tool in detail. The amplitude of the reflected acoustic pulse can be plotted on a 3-axis oscilloscope as a function of beam azimuth and vertical position in the hole, producing an image of

well-bore reflectivity or "smoothness." As the tool is moved vertically in the hole (at a rate of about 2.5 cm/s, a photograph of the traces on the scope yields a 360° image of the vertical section of the wall. Hard, smooth surfaces producing high-amplitude reflectance result in white zones in the image. Fractures, voids, and soft ma-

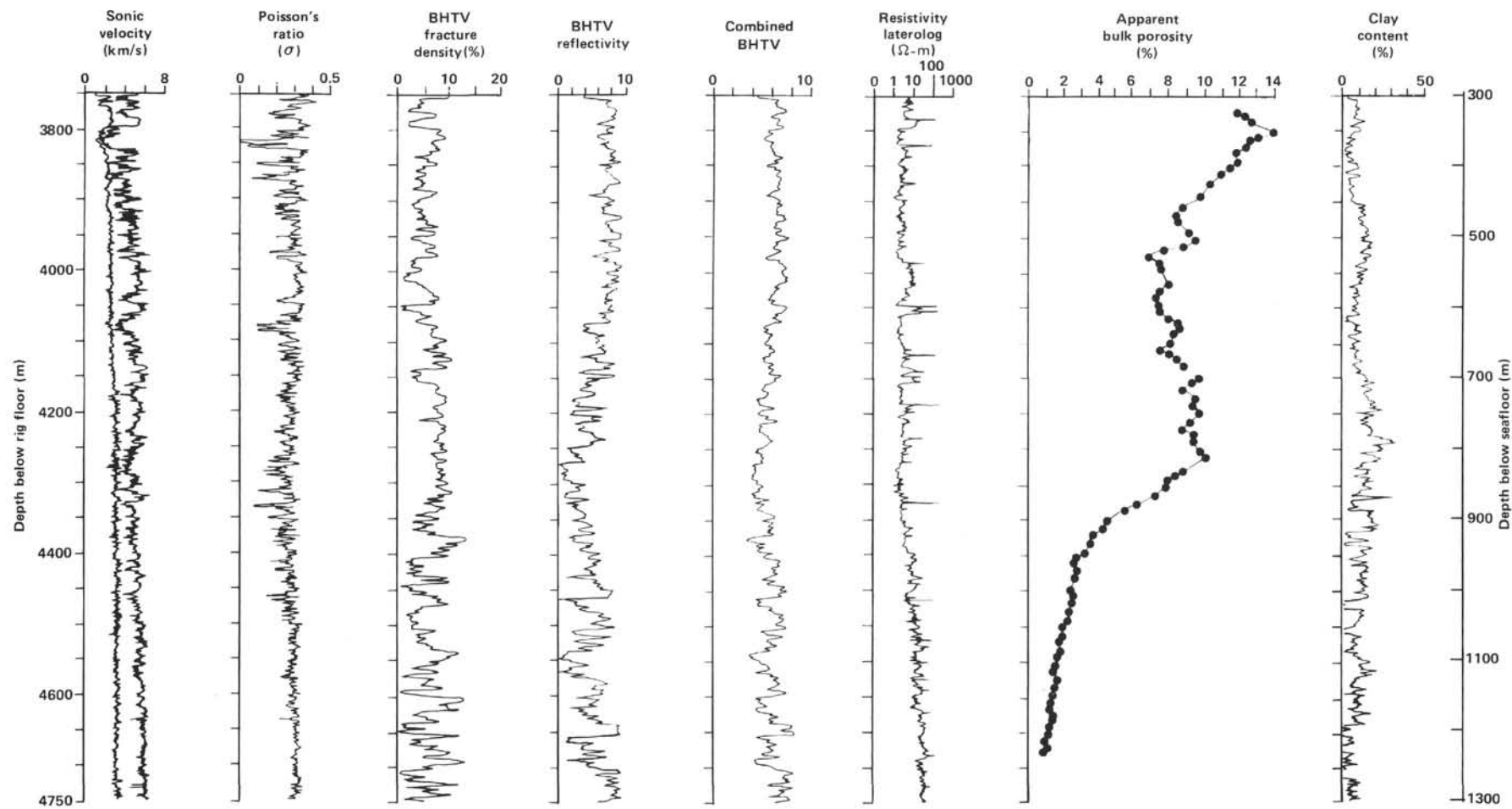


Figure 2. Geophysical logs down Hole 504B. Note changes at Layer 2A/2B and 2B/2C boundaries, 3850 and 4400 m below rig floor (376.5 and 926.5 m BSF), respectively. See text for discussion.

terial that absorb or scatter much of the signal produce low-amplitude reflectance or dark zones in the image. A fluxgate magnetometer in the tool triggers the scope trace at magnetic north so that the orientation of observed features can be determined.

Resolution of the tool depends on hole diameter, wall conditions, reflectivity of the formation and acoustic impedance of the wellbore fluid. For Hole 504B, the optimum resolution (excluding such factors as ship's heave and changes in the acoustic impedance of the wellbore fluid with depth and temperature which would degrade the resolution) is 0.17 cm per firing (horizontal) and horizontal/vertical resolution ratio of 0.20. Fractures with apertures less than 1 cm can be distinguished.

The BHTV records from Hole 504B are degraded by the effects of ship's heave during logging. This causes the tool to either stand still briefly or to be pulled up or dropped down at a higher rate than the normally slow logging speed it requires. This causes vertical streaks in the record, up to a third of a meter in downhole depth (Hole 504B summary chapter, this volume).

Because of the extreme temperature changes encountered in the hole, the compass triggering circuit in the tool occasionally misfired. This shows up as a horizontal line of data that continues to the right margin of the photographs of the images, such as found between 4430 and 4432 m below the rig floor (956.5 and 958.5 m below seafloor, BSF). The overall loss of data that is due to this misfiring is quite small.

There is general dark-light banding running vertically down the records. This results from the tool being off-center in the hole, a consequence of the small-sized centralizers with which the tool is equipped (Hole 504B summary chapter, this volume). Thus, the records appear lighter in the direction of the nearest wall and darker toward the far wall. In addition, there is a more distinct

vertical banding in intervals of borehole breakout (see Newmark, Zoback, and Anderson, this volume).

In Figure 3, we can see examples of the three main lithologic types found in the BHTV records from Hole 504B. Toward the left is an example of a pillow basalt unit with a line interpretation of its major features for clarification. There is a horizontal exaggeration of about 3:1. Pillow units can be distinguished by the appearance of horizontally-oriented ellipsoidal bodies, usually with bright reflective centers, outlined by dark rims, indicating lower reflectance. They are often up to a meter across (about the width of the photograph) and up to a third of a meter high. They are often cut by numerous shallow-dipping cracks and voids and tend to have a generally mottled appearance in the record. When a planar feature such as a fracture plane intersects the borehole at dip angles between 0 and 90°, a distinct sinusoidal pattern will be seen. The steeper the dip, the more elongated the nose of the peaks. However, because of the considerable horizontal exaggeration in these BHTV records, fractures and other planar features appear to have significantly shallower dips than they actually have. Pillow units are not found below 4520 m (1046.5 m BSF).

Massive units are distinguished by their solid texture and the relative absence of voids and cracks. Since the BHTV records high-amplitude reflections as light, massive units are very bright in the records.

Brecciated units are distinguished by their generally dark and chaotic appearance in the records. They look much like pillow units except they appear to have a more regular texture, are generally darker, and pillows are absent in them (Hole 504B summary chapter, this volume).

A detailed discussion of the lithostratigraphy seen in the BHTV records obtained in Hole 504B can be found in Appendix A. The general structure revealed by the BHTV records can be summarized as follows: Layer 2A

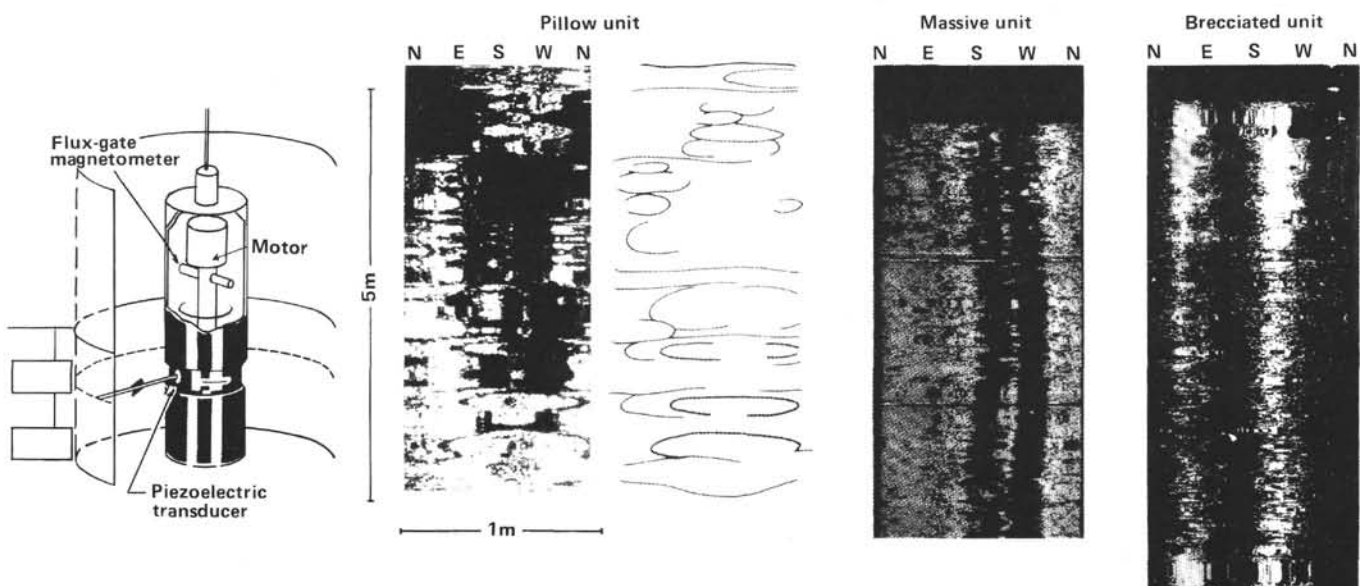


Figure 3. On the left is a schematic diagram of the borehole televiewer (after Zemanek et al., 1970). To the right are examples of the three dominant lithologic types found in the BHTV records — a pillow basalt unit with a line interpretation of its major features, a massive unit, and a brecciated unit. See text for discussion.

(the upper 100 m of basement) is composed of mostly thin flow units and pillow basalts. The average pillow diameter and flow thickness decreases with depth, although large-diameter pillows and thicker flow units are not uncommon. Layer 2B (the middle 550 m of basement) is chiefly composed of thin flows and small diameter pillows. Fracturing is pervasive and zones of brecciation are common. Layer 2C (the lower 350 m of basement) is composed mainly of massive, "welded" units, although a few pillows appear above 4520 m (1046.5 m BSF). It is generally less fractured than the overlying section.

Borehole Televiewer Logs

There are three logs or records of the downhole variation of some physical property that can be quantified from the BHTV records. These are seen along with other logs in Figure 2. The first is a fracture density log. This is determined by estimating the percentage of fractured material in each downhole meter of the BHTV images, where each meter overlaps the previous one by a half meter. Thus the fracture density log involves a running average with an offset of a half meter. In Figure 2, the fracture density log is averaged with a 10-m running average for clearer presentation. Void spaces are not included as areas of fracturing, but breccia zones are. The major source of error in these estimates is that due to ship's heave, which produces zones in which no estimate can be made. It is not considered to be a large effect.

A second log is a measure of BHTV reflectivity, which is an indirect measure of the void space in the borehole wall. This is determined by measuring the overall reflectivity of the BHTV images with a light meter every half meter. The values range from 0 to 10, which is the dynamic range of the light meter used. In Figure 2, this log is averaged with a 10-m running average for clearer presentation.

The combined BHTV log is a qualitative estimate of the presence of both fractures and void space in the hole. It is determined by combining the fracture density and reflectivity logs so that it has low values in sections with a high fracture count and low reflectivity, and high values in more solid rock with high reflectivity and low fracture count. In Figure 2, this log is averaged with a 10-m running average for clearer data presentation. The combined BHTV log is scaled so that zone of massive, unfractured rock will yield a value of 10, and complete absence of reflected energy will yield a value of 0. Thus this log is a relative measure of the competence of the wall rock.

Fracture Orientation

The BHTV records show that fracturing is predominantly shallow-dipping (usually less than 30°), throughout the hole.³

³ It is important to note that the fractures seen by the BHTV are macrocracks that are large (on the order of equal to or less than 1 cm) compared to those found in most hand specimens. The fractures seen in hand specimen from the core barrel are generally too small to be seen by the BHTV, and are of random dip (Natland, personal communication, 1983).

This same predominance of horizontal to subhorizontal fractures was observed in the upper part of the hole by Zoback and Anderson (1982). A vertical borehole that samples even a set of randomly oriented fractures will preferably encounter more horizontal to subhorizontal than vertical to near-vertical ones. We attempted to quantify the apparent horizontality of the fractures in the hole by comparing the observed crack orientations to a model in which a field of randomly oriented cracks is penetrated by a vertical borehole.

We calculate a curve in which the number of cracks intercepted by a borehole is shown as a function of the dip of the cracks (Fig. 4A). This curve was calculated using a random-angle model, whereby a vertical borehole 5 m long and 25.4 cm in diameter intercepts a field of cracks evenly spaced at 10-cm intervals, with dips ranging from 0 to 90°. The 10-cm spacing was chosen as this was the smallest common crack spacing counted in the analysis of the records from Hole 504B. The model uses infinite length cracks and thus predicts the largest possible number of cracks encountered. The curve has a distinct cosine form.

Cracks seen in the BHTV records with apertures equal to or greater than 1 cm were counted and their dips were measured in some 41 5-m-long intervals evenly spaced over the length of Hole 504B. The dips of the fractures were measured to ±5° by comparing the observed fractures on the images with sample fractures of different dips outlined on a clear overlay for which the horizontal exaggeration of the images was taken into account. The intervals analyzed occur every 20–30 m and account for approximately one fifth of the total hole depth. Plots of the number of cracks encountered in these intervals in each of the crustal layers plotted versus dip (Fig. 4B) clearly show that the fracturing is not random. The number of cracks encountered in the crustal Layers 2A, 2B, and 2C reflect the proportion of the hole that penetrates these layers. (Thus the curve for the pillows [Layer 2A] has the lowest count, and the curve for Layer 2B has the highest.) Curves for the number of cracks encountered in each layer normalized to 50 m are also shown in Figure 4B. Despite the differences in their peak values, the important point is that none of these curves resembles the cosine form of the frequency curve that is predicted for a vertical borehole intersecting a field of fractures with dips showing a random distribution. There is a gross predominance of horizontal-to-shallow-dipping fractures. The likelihood of encountering cracks with dips from 40 to 90° is nearly constant. There is a slight increase in total number of cracks with dips from 80 to 90° suggesting that the crack distribution is bimodal. However, this increased value at high dip angle approaches the predicted value for a uniformly oriented fracture set and is probably not a significant change. The overwhelming presence of subhorizontal features encountered by the BHTV and the near absence of moderate-to-steeply-dipping fractures indicates that the dominance of subhorizontal structures is real and of geological significance.

It may be argued that the dominance of subhorizontal features in the BHTV records is a result of an inher-

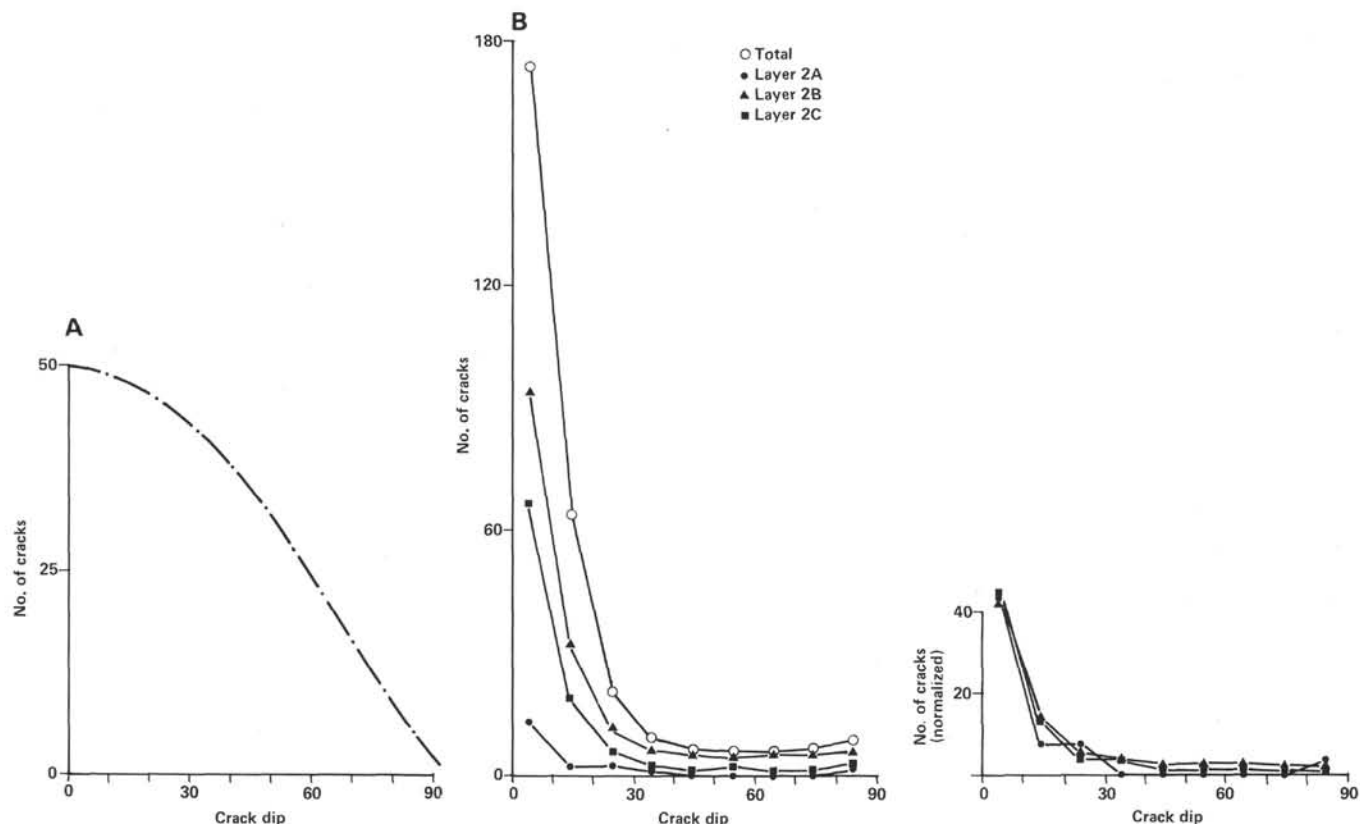


Figure 4. A. A calculation of the maximum number of cracks encountered by a vertical borehole in a randomly oriented field of cracks, plotted versus crack dip. In the model, a 5-m-long, 25.4-cm-diameter vertical borehole intercepts a field of cracks evenly spaced at 10-cm intervals, with dips varying from 0 to 90°. Note the cosine form of the curve. B. The number of cracks counted in 41 5-m-long intervals evenly spaced with depth down Hole 504B as seen in the BHTV images plotted versus crack dip. The individual curves indicate the total number of cracks for all intervals (triangles), the cracks encountered through Layers 2A (dots), 2B (crosses), and 2C (plusses). The number of cracks counted in each layer reflects the depth interval of each layer. Thus, there are relatively fewer cracks counted in Layers 2A and 2C than in Layer 2B. C. Same data normalized to a layer 50-m thick. Total number of cracks per normalized 50 m in each layer are 63 (2A), 73 (2B), and 67 (2C).

ent horizontal bias in the BHTV imaging system. The BHTV has been used extensively on land in hydraulic fracture experiments and has been shown faithfully to record steeply dipping and vertical features in a borehole *when they are present* (Seeburger and Zoback, 1982). We believe that the distribution of macrocrack orientations found in the BHTV records is a true representation of the orientation of these structures in Hole 504B. This implies that the formation may respond as a strongly anisotropic medium with a vertical, rather than lateral form of anisotropy. If so, this anisotropy will affect the P and S velocities.

LOGGING DATA AND POROSITY

Comparison of several of the geophysical logs with the BHTV log can yield some insight into the physical causes for the changes in seismic velocity with depth.

In Figure 2, we see the sonic velocities plotted with depth. Downhole logging of both P and S velocities allowed us to make a continuous calculation of the V_p/V_s ratio and an estimate of the dynamic Poisson's ratio, which is also shown. This is particularly important since Poisson's ratio is sensitive to both the extent and nature of porosity, which will be discussed later.

The three logs derived from the BHTV records are shown in Figure 2. Results from both the downhole resistivity log and the large scale resistivity experiment are also shown. The apparent bulk porosities calculated from the resistivities are plotted for the large-scale resistivity experiment. The resistivity values generally followed the trends shown in the downhole resistivity log (Becker et al., 1982; Becker this volume). These two experiments differ primarily in the depth of formation sampled by each one; the spherically focused laterolog samples about 0.5 m into the formation, whereas the large-scale resistivity experiment penetrates many meters into the formation, and averages over larger sample paths (Becker et al., 1982; Becker, this volume).

Also shown in Figure 2 is a prediction of clay content determined by cross-correlating the nuclear logs, particularly the porosity-sensitive gamma-ray density and the hydrogen-ion-sensitive neutron-porosity logs (Anderson, O'Malley, and Newmark, this volume). The signals of each of these logs respond differently to the presence of rock, pore fluid, and chemically bound water. The processing attempts to distinguish between "free" water and "bound" water that is associated with clays and is therefore not free to move. This log qualitatively agrees with

the amount of alteration present in the recovered cores. However, since the percentage of core recovery is so low in this hole, this log provides more continuous information about the abundance of hydrated minerals down-hole than would otherwise be available.

Layers 2A, 2B, and 2C in Hole 504B have been based on the seismic character and the velocity gradients. Similar gradient changes have been seen in the other geophysical logs also.

The uppermost 100 m of basement (Layer 2A) is an aquifer of rubbly pillow basalts, breccias, and a few massive flows (CRRUST, 1982). Here we see variable but generally low P and S velocities. Poisson's ratio is quite high. Resistivity decreases, then increases as apparent bulk porosity increases, then decreases over this section.

The next 550 m show moderate velocity gradients and decreasing Poisson's ratio accompanied by increasing fracture density, decreasing BHTV reflectivity, and variable but slightly decreasing resistivity values. The combination of increasing fracture density and decreasing reflectivity attests to the extensive brecciation over this section, interpreted to be seismic Layer 2B. The apparent bulk porosity fluctuates between 6 and 10%. In addition, the bulk formation permeability drops by more than an order of magnitude over this interval (Anderson, Zoback, et al., this volume). The recovered material shows this section to contain the highest proportion of hydrated minerals in the hole, which confirms the prediction of high clay content in the clay content log.

At 4390 m (916.5 m BSF) sharp changes occur in many of the geophysical properties. This is perhaps most strikingly seen in the two resistivity logs (resistivity laterolog and apparent bulk porosity from the large-scale resistivity experiment), but also is mirrored in most of the others. The electrical resistivity shows a slope change to higher gradient, and apparent bulk porosity drops. P-wave velocity begins a steady increase, as does Poisson's ratio. Fracture density begins to fluctuate between about 0 and 12. Combined BHTV begins a gradual increase. Other parameters change as well (Anderson et al., 1982): for example, sample thermal conductivities show a step-wise increase of ~25% (Anderson et al., Becker, both this volume). These changes in geophysical properties occur in the section of the hole that has been interpreted to be the Layer 2B/2C transition on the basis of the recovered cores. Here, the transition is much sharper than the one defined by petrologic evidence alone.

The lower 350 m of the hole, interpreted to be seismic Layer 2C, shows moderately increasing P and nearly constant S velocities. Fracture density is variable, but lower on the average than in the overlying section. BHTV reflectivity is variable but generally increases. Both Poisson's ratio and resistivity steadily increase with depth. The increasing resistivity indicates a decrease in bulk porosity. The prediction of low clay content in this section agrees well with the low bulk content of hydrated minerals observed in the recovered cores. In fact, the change at 4390 m (916.5 m BSF) shows up as about a 10% drop in alteration pervasiveness below versus that occurring above (Alt et al., this volume).

The presence of open, water-filled cracks in a formation will affect the compressional and shear velocities differently. Since shear waves will not propagate through a fluid, the shear wave velocity will be highly affected by the presence of water-filled cracks. However, if the cracks are filled with a relatively low-density material such as clay, the propagation of shear waves will be less affected, and thus the ratio of compressional to shear velocity will be quite different. As a measure of the V_p/V_s ratio, Poisson's ratio is sensitive to the presence and character of large-scale porosity in a formation.

In Figure 5, we can see compressional velocity, fracture density, combined BHTV, and clay content plotted against Poisson's ratio with increasing depth in Hole 504B. These data represent 50-m averages.

In Layer 2A (the upper 100 m of basement), Poisson's ratio decreases with increasing compressional velocity. This can be explained by the predominant effect of large, open fractures and void spaces as demonstrated in the plot of fracture density versus Poisson's ratio (Fig. 5B).

In Layer 2B (the middle 550 m of basement), V_p is nearly constant but V_s changes, causing Poisson's ratio to increase and then decrease. In the plots shown in Figure 5, we can see the effect of increasing, then decreasing bulk content of hydrated minerals. The overall fracture density increases, and the clay content plot indicates that these fractures are filled with clay. The combined BHTV plot shows that the overall competence of the wall rock decreases through this section.

In the lowermost section of the hole (Layer 2C), Poisson's ratio increases with increasing V_p . Fracture density decreases and the combined BHTV log shows that the overall competence of the wall rock increases. The predicted clay content decreases through this section.

Discussion

In measurements on laboratory samples, Hyndman (1979) found that grain boundary, or large-scale porosity in the form of open, water-filled cracks, results in lower seismic velocities and high Poisson's ratios (>0.30), whereas vesicular or poorly interconnected porosity such as that found in highly altered zones results in lower Poisson's ratios (>0.30). His data are shown in Figure 6 in the form of Poisson's ratio plotted against compressional velocity. The results are based on laboratory measurements on small samples, but the general influence of open or filled cracks on the propagation of compressional and shear waves on the microcrack scale should be similar to the influence of larger, open and filled cracks in the wall rock formation. However, if there is significant vertical anisotropy in the wall rock of Hole 504B (see section on fracture orientation), any comparison between our data and Hyndman's may be invalid.

In Layer 2A (the upper 100 m of basement), the observed slope in Poisson's ratio versus compressional velocity plot (Fig. 5A) coincides with the high fracture density and low predicted clay content. This could be a result of grain boundary or open porosity (Hyndman, 1979). In Layer 2B (the middle 550 m of basement), the

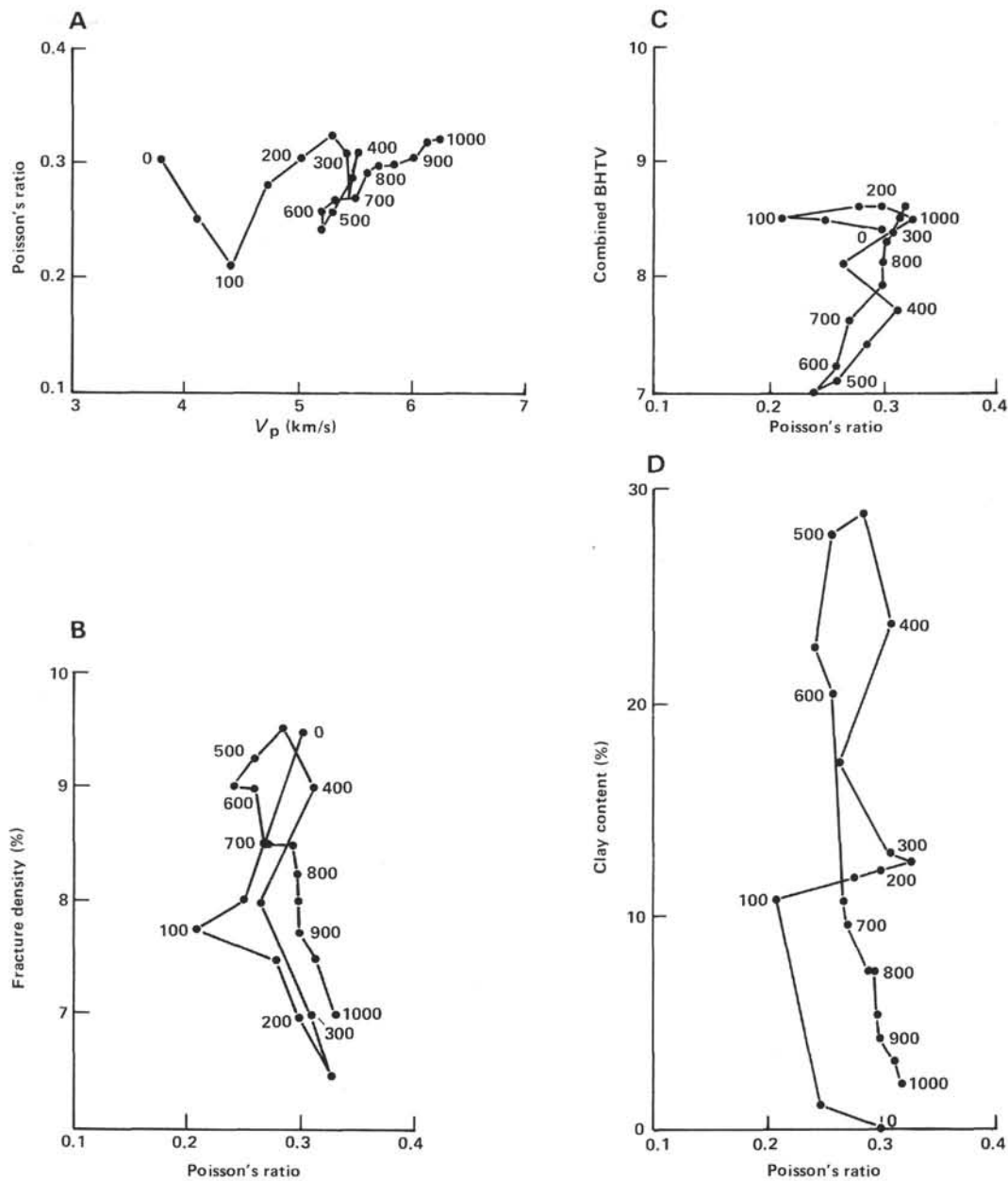


Figure 5. Values of Poisson's ratio from Hole 504B are plotted versus (A) compressional sonic velocity (V_p), (B) BHTV fracture density, (C) combined BHTV, and (D) clay content prediction. Numbers refer to depths below the rig floor in meters. (A) is plotted for direct comparison with Hyndman's (1979) data (see Fig. 6). Note the changes in slope signifying different relationships between these properties in Layers 2A (3750–3850 m), 2B (3850–4400 m), and 2C (4400–4750 m) (276.5–376.5, 376.5–926.5, and 926.5–1276.5 m BSF, respectively).

slope changes in the plot of Poisson's ratio versus compressional velocity (Fig. 5A) coincide with the changing predicted clay content and high fracture density. This could be the result of vesicular porosity or of plugging of fractures with alteration products (Hyndman, 1979). In Layer 2C (the lower 350 m of basement), the increasing Poisson's ratio with increasing compressional velocity (Fig. 5A) coincides with decreasing fracture density and predicted clay content. Hyndman's (1979) model would predict that the observed slope in Figure 5A is a result of vesicular porosity or of plugging of fractures with alteration products. However, this cannot be the case as our predicted clay content sharply *decreases* in

the bottom part of the hole, and the recovered basalt contained a very small bulk content of hydrated minerals, especially as compared to the material recovered from Layer 2B.

O'Connell and Budiansky (1974) have proposed a model whereby saturation and degree of cracking are related to effective Poisson's ratio and shear velocity in a cracked solid and that is in general agreement with Hyndman's data. Figure 7 shows the O'Connell and Budiansky (1974) model with our data plotted as a function of depth into basement. We see the decrease in fracturing and Poisson's ratio in Layer 2A, the increase and subsequent decrease through Layer 2B and the increase

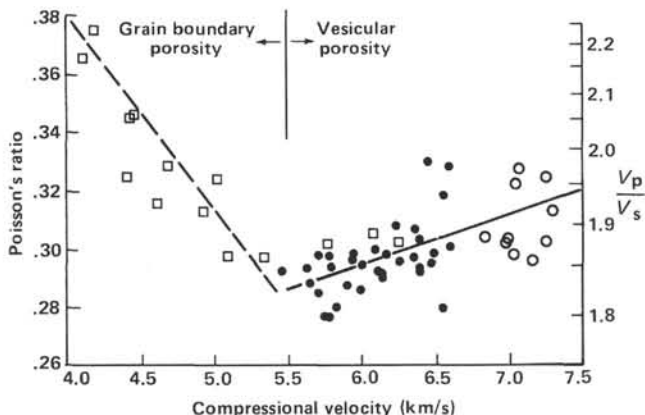


Figure 6. The effect of porosity on Poisson's ratio for subaerial mainly pyroclastic samples from the Azores (open squares) and for DSDP Leg 37 fresh deep-sea basalts (solid dots) and gabbros (open circles) from the Mid-Atlantic Ridge. Note the opposite dependence of Poisson's ratio on porosity, grain boundary, and vesicular porosity (from Hyndman, 1979).

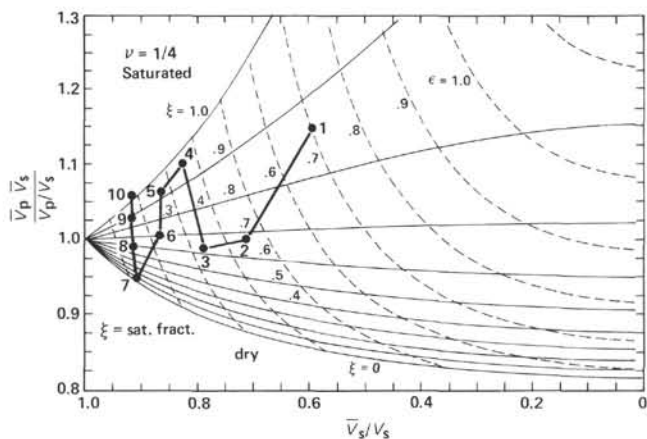


Figure 7. O'Connell and Budiansky's (1974) model for fracture density (dashed curves) with variable porosity (water saturation, solid curves). Hole 504B effective V_p/V_s versus effective V_s is plotted every 100 m downhole, so 1 = 100 m into the oceanic crust, etc. Arrows point toward data downhole.

in Poisson's ratio with nearly constant shear velocity in Layer 2C. The relationships in Layers 2A and 2B are clearly explained by this model, but not, the results through Layer 2C. Here the model would predict an increase in fracturing and thus an increase in saturation to explain the observations in Layer 2C. However, the BHTV fracture density *decreases* through this section, and the increase in resistivity indicates a distinct decrease in porosity through this section of the hole.

The present models would predict the lower part of the hole to be either highly altered or more intensely fractured than the overlying unit, and it is neither. Thus, we seek a new model to explain the observations in this lowermost section of the hole.

A series of gross changes in the nature of porosity and values of Poisson's ratio with depth in the hole have been described. These changes have been shown to

occur over relatively large (>100 m) depth intervals. Another type of relationship has been found in the geophysical logs that indicates changes in some of the physical properties over much shorter intervals. These will be discussed in the next section.

LOGGING DATA AND FRACTURE CYCLICITY

In analyzing the geophysical logging results, it was observed that several of the downhole logs seemed to "track" each other down the hole with a periodicity of some 10 to 50 m. This is particularly apparent in the neutron density, porosity, electrical resistivity, sonic, and BHTV logs. Figure 8 shows a 75-m section of these logs where a general rise and fall is exhibited with a periodicity of 15 to 30 m. Although the greatest amplitude of variation is in the BHTV fracture density log, this periodicity cannot be a result of ship's heave, cable resonance, or subjective interpretation since these effects occur on a 1-m wavelength, and the observed periodicity involves wavelengths of many times this amount. Since the sonic, resistivity, and BHTV logs are most sensitive to the presence of fractures and open porosity, we concentrated our analysis on these logs. Phase difference analyses were carried out between the P-wave, electrical resistivity, and combined BHTV logs in order to quantify these apparent correlations.

In a phase difference analysis, each signal is first Fast-Fourier-Transformed. This provides a breakdown of the relative amounts of energy at different frequencies that contribute to the entire signal. The "frequency" is really 1/wavelength along the hole, or depth. Then the two signals to be analyzed are compared to determine if they are both in phase at each frequency. The phase difference is a measure of the percentage of energy in phase between the two signals at a particular frequency. If both signals are completely in phase at a particular frequency, a value of 1.0 (or 100% of the energy in phase) is displayed; if the signals are 180° out of phase, the value is 0.0 (or no energy in phase), if they are out of phase by 45°, the value is 0.85, and completely random signals would produce an average difference of 0.5. [See Appendix B for derivation of phase coherence, $D(\omega)$.]

The results of the phase difference analyses between the P-wave, electrical resistivity, and combined BHTV logs are shown in Figure 9. These plots indicate the percentage of energy of both logs in phase at a particular frequency along the entire length of the hole. They give no information regarding the section of hole in which the logs are in phase at each particular frequency. The majority of the signals are in phase at the wavelengths appropriate to this discussion, which are from 10 to about 100 m. Wavelengths smaller than 10 m have little significance since they approach the thickness of the individual flow units in the upper part of the hole. We are mainly interested in periodicities that seem to be associated with longer wavelengths, or periodicities involving many individual units with depth. Wavelengths much larger than 100 m are not significant as they approach the thickness of Layers 2A, 2B, and 2C, which we would expect to have a different character. Also, larger wave-

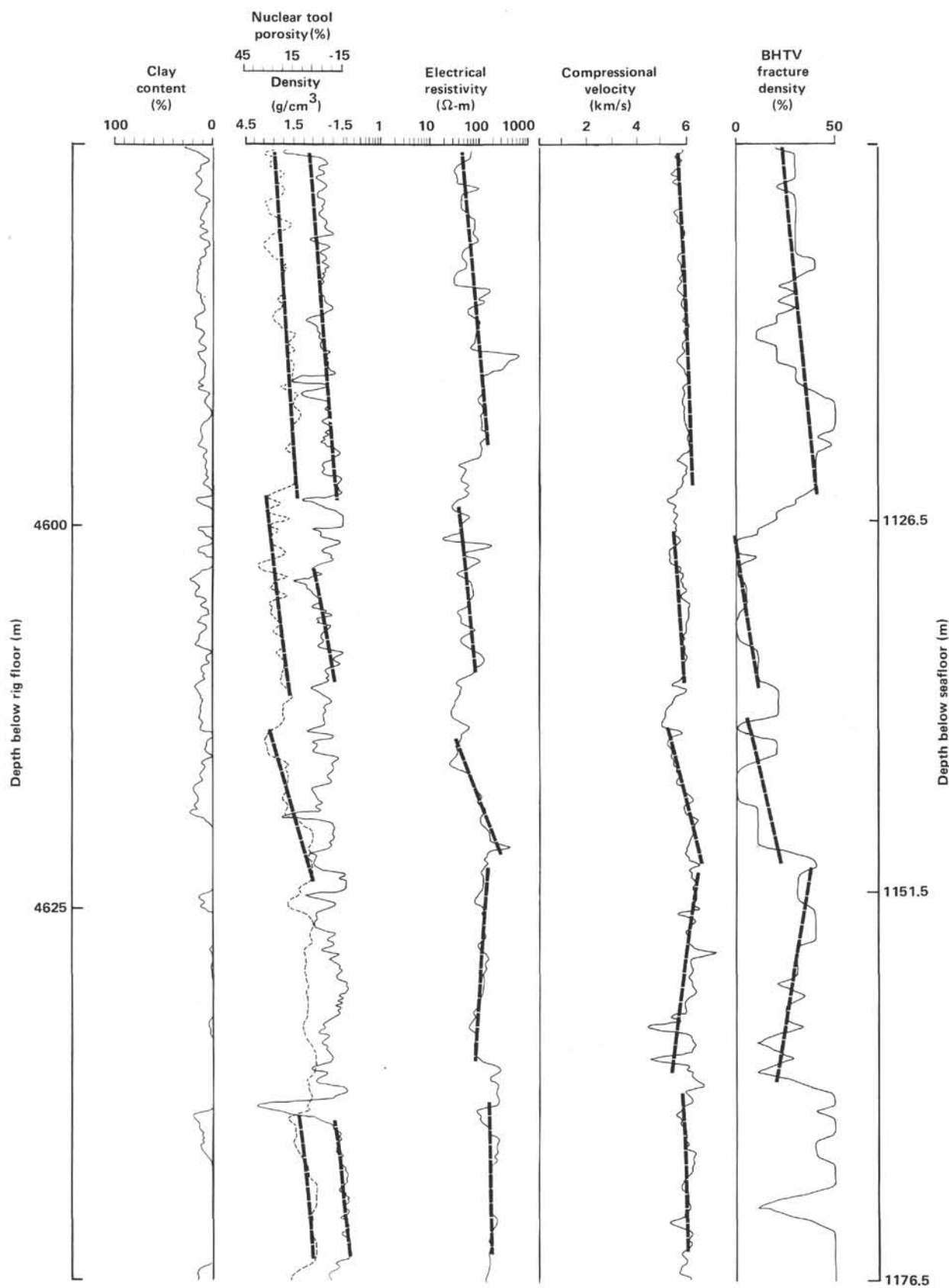


Figure 8. Megalog from Hole 504B in dikes at 4575–4650 m depth below the rig floor (1101.5–1176.5 m BSF). From left: predicted clay content log in percent from 0 to 100%, nuclear tool density (dashed) and porosity (solid), electrical resistivity from the spherically focused laterolog, compressional velocity, and borehole televiewer fracture density log. Heavy dashed lines emphasize similar “rising” and “falling” trends in the data.

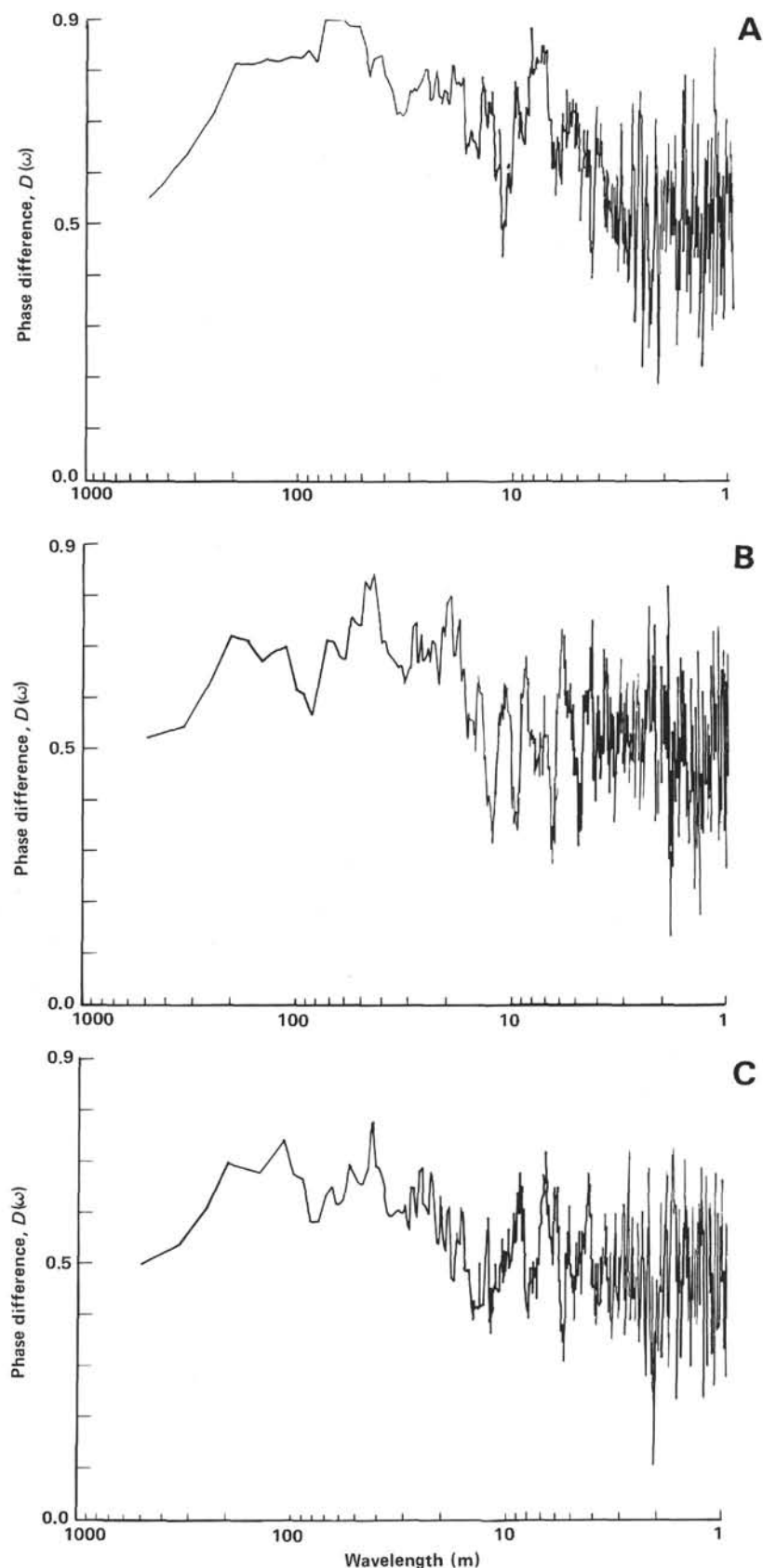


Figure 9. Phase difference analyses of (A) compressional sonic velocity vs. electrical resistivity, (B) electrical resistivity versus borehole televiewer, (C) compressional sonic velocity versus borehole televiewer. Note the bands of highly coherent energy between 10 and 100 m.

lengths become significant fractions of the length of the hole, and phase difference analysis of such long wavelength signals would have no scientific value.

High values of phase difference (Fig. 9) indicate that a strong cross-correlation exists between the compressional sonic velocity, electrical resistivity, and fracture density so that zones of high fracture density correlate with low sonic velocity at wavelengths ranging from 10 to 100 m. Moreover, these plots indicate different wavelength ranges in which there is particularly coherent energy. This means that strong correlations exist between these signals within these wavelength bands somewhere in the hole.

To insure that these apparent relationships were not due to improper compensation of the logs for local variations in the borehole size (the sonic and resistivity tools were borehole compensated), phase difference analyses were run between these logs and the caliper log (Fig. 10). At wavelengths less than about 50 m, the energy seems to fluctuate around 0.5, which indicates a generally random phase relationship. In all three cases, the longer wavelengths indicate that the energy is out of phase. For the P-wave versus caliper plot, this can be explained as the response of the logs to the long-wavelength change at the bottom of the hole where the overall hole size decreases, while the P-wave velocity increases. In the shallower sections, relatively large hole diameter coincides with lower P-wave velocities. This long-wavelength relationship is not an indication of improper borehole compensation by the sonic tool. In the televIEWer versus caliper plot, the long-wavelength relationship is also a result of the overall decreasing hole diameter with depth. In the shallow section, the larger hole diameter results in lower overall reflectivity, whereas in the bottom of the hole, the smaller average diameter results in relatively higher reflectivity. Again, for the resistivity versus caliper plot, the long-wavelength relationship can be explained as a coincidence of the overall decreasing hole diameter with an overall increase in resistivity as a result of decreasing porosity. These changes occur at longer wavelengths than the periodicities we have observed.

Similarly, there is no apparent correlation between these relationships and the core intervals or drill bit changes, either of which might result in an abrupt change in loading at the bottom of the hole, and thus might produce fractures. The peaks and troughs of the apparent signals are neither coincident with depths at which the drill bit was changed, nor with the depths of coring intervals. These relationships are not an artifact of the drilling process. Thus we can assume that they are real and of geologic significance.

Next, the signals from the logs were bandpassed in each of the three wavelength bands in which high values of phase difference were identified: 100–30, 30–20, and 20–10 m. This allows a comparison between the variations in amplitude of the three signals at a particular range of wavelengths and gives a visual description of the correlations identified by the phase difference as a function of depth.

The results of the bandpass from 100 to 30 m are shown in Figure 11A. To the left are the three signals — V_p , resistivity, and combined BHTV — plotted versus depth. To the right is a running average of the percentage of all three signals in phase down the hole. The three signals are compared in three pairs, such that for each pair, for every 0.5 m down the hole, if the two signals are in phase, a value of 1 is given. If they are out of phase, a value of 0 is given. Thus, for each depth of measurement, the sum of the values can be 0, 1, 2, or 3, where 0 indicates that none of the signals is in phase with another and 3 indicates that all three signals are in phase. These values are then averaged with a 10-m running average and normalized to 0 to 100% in order to produce the curve on the right of Figures 11A–C. For example, at about 400 m BSF, there is no strong relationship shown between the three signals at longer wavelengths (100–30 and 30–20 m), (Figs. 11A, B), but there is some moderate level of energy in phase at the shorter wavelengths of 20–10 m (Fig. 11C). By comparison, at about 600 m BSF, there is a large amount of energy in phase at longer wavelengths of 100–30 m (Fig. 11A), but only a moderate amount of energy in phase between the three signals at the shorter wavelengths of 30–20 and 20–10 m (Fig. 11B, C). It is apparent that there are several intervals where all three signals are in phase and the energy is coherent at these wavelengths in the hole. The longer wavelengths are particularly coherent in Layer 2C (below 926.5 m BSF). Note that many of the obvious coherent energy packets seem to occur at a wavelength of about 50 m.

The results of the bandpass filtering from 30 to 20 m are that although there are a few sections of the hole showing coherence at these wavelengths in the shallow section, the lower part of Layer 2B and the upper part of Layer 2C seem to be most strongly coherent at these wavelengths (Fig. 11B).

Although it is difficult to discern the individual signals in the 20–10 m bandpass interval, the average plot to the right indicates that throughout the hole there is some coherence at these wavelengths (Fig. 11C).

Discussion

The dominant subhorizontal features in the upper part of the hole can be interpreted as being flow-parallel fractures related to the cooling of subhorizontal flow units in Layers 2A and 2B. In fact, because of the diffuse nature of some of these features, it is possible that a few of the features considered to be fractures in the upper part of the hole may actually be flow tops or bottoms wrongly identified. However, this interpretation cannot explain the presence of the subhorizontal features in the dikes of Layer 2C. These are usually quite distinct in character and cannot be interpreted as contact zones. The continuing dominance of subhorizontal features in the dikes of Layer 2C is more difficult to explain.

In ophiolites, the average dike width is approximately 1 m, although measured dike widths range from a few tens of centimeters to several meters (Fox and Stroup,

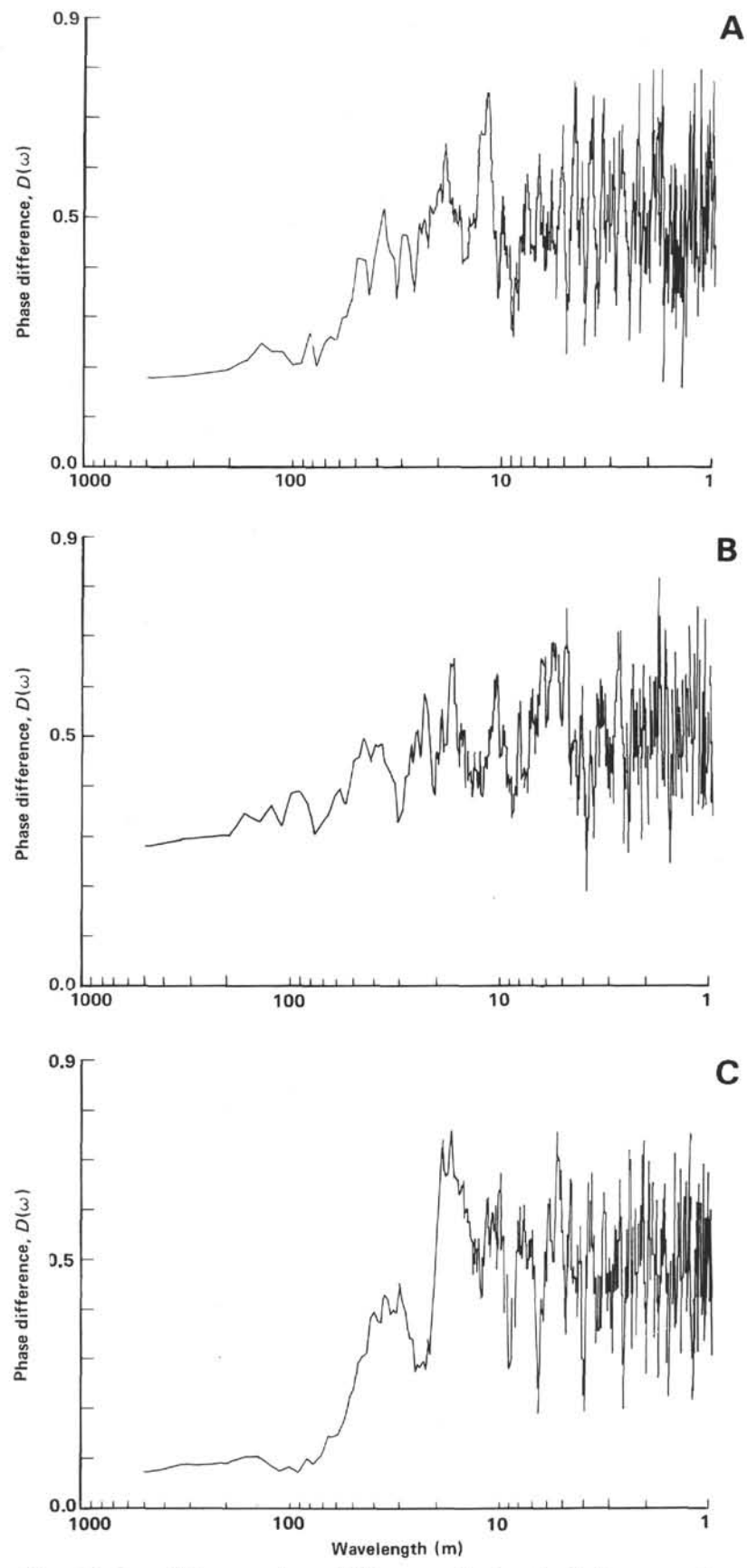


Figure 10. Phase difference analyses of (A) compressional sonic velocity versus caliper, (B) borehole televiewer versus caliper, and (C) electrical resistivity versus caliper. Note that much of the energy fluctuates about 0.5 between 10 and 100 m.

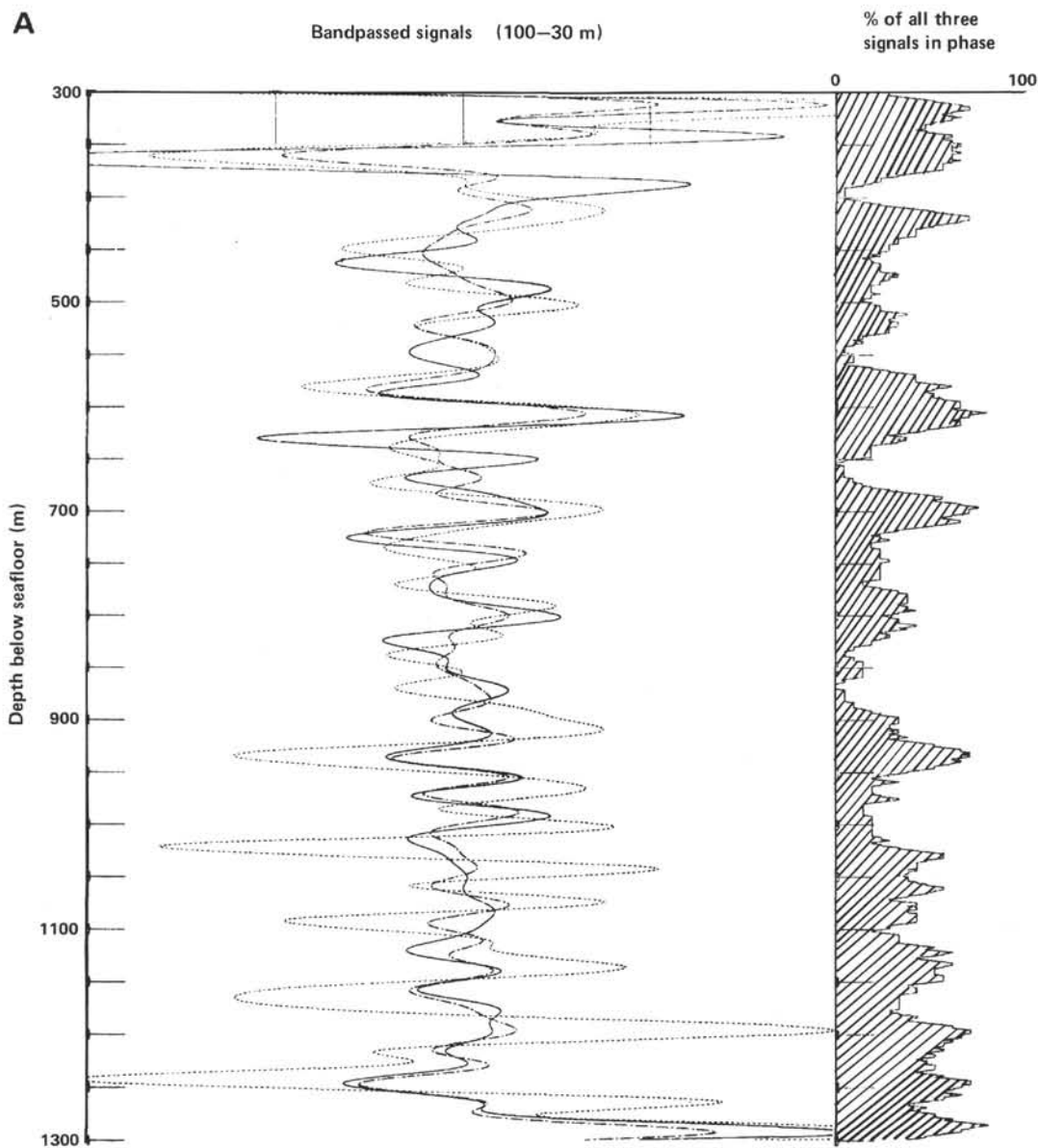


Figure 11. The three signals, compressional sonic velocity (solid), electrical resistivity (dashed), and borehole televiewer (dotted), bandpassed at (A) 100–30 m, (B) 30–20 m, and (C) 20–10 m, plotted versus depth. To right, the percentage of all three signals in phase versus depth, averaged every 20 m. Note the dominance of signal energy in phase at intermediate (30–20 m) wavelengths through the lower part of Layer 2B and the upper part of Layer 2C (4200–4550 m below the rig floor), and the dominance of signal energy in phase at longer (100–30 m) wavelengths at the bottom of the hole through layer 2C (4400–4750 m below rig floor).

1981; Casey et al., 1981). Massive flows of the volcanic carapace of ophiolites range in thickness from a few centimeters to several meters (Casey et al., 1981). For example, the majority of the massive flows of the North Arm Massif, Bay of Islands, ophiolite in Newfoundland, are between 15 cm and 1 m thick, although they range in aspect from lenticular flows a centimeter or two thick to massive flows several meters thick (Rosencrantz, 1983). In general, the individual intrusive and extrusive units that form the upper part of the oceanic crust are on the order of 1 m thick. Analysis of the recovered cores and downhole geophysical logs from Hole 504B has shown that the thickness of the individual cooling units is simi-

larly on the order of 1 m, with a few rare, thick, massive units as large as 10 m thick (Adamson, this volume; CRRUST, 1981; Zoback and Anderson, 1982). There is no evidence of petrologic variation with depth at any wavelengths in this hole (Emmermann, this volume). The apparent periodicity seen in some of the geophysical logs is not a result of petrologic or lithologic variations with depth in the hole.

The next question is whether or not these features, when encountered in the dikes of Layer 2C, are subhorizontal cooling joints. In naturally occurring tension crack systems such as the cooling joints in basaltic lava, the crack depth should be of the same order of magnitude

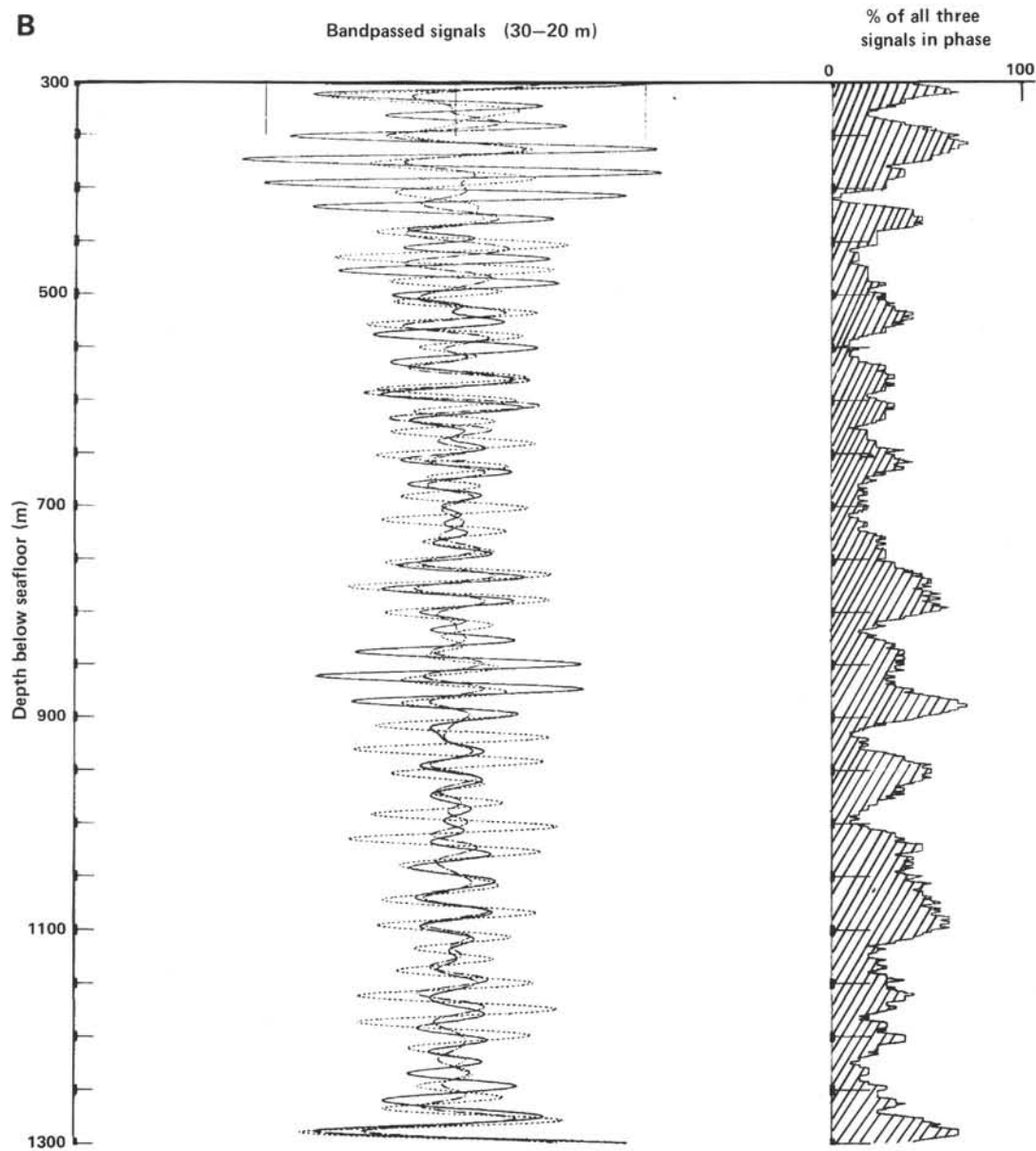


Figure 11. (Continued).

or less than the crack spacing (Lachenbruch, 1961). Otherwise, neighboring cracks would be initiated in zones of greatly reduced tension. It is unlikely, therefore, that cooling-induced joints would only be found spaced at intervals of 50 m or more in dikes only a meter or so wide. What is more likely is that the features we are seeing are caused by some other mechanism besides normal cooling-induced joint formation, but the presence of cooling-induced joints or weaknesses in the dikes provides a preferred pathway for further crack opening under an induced stress. By a negative comparison, if these features are actually joints in the dikes, then why do we not see subvertical joints in the massive flows in the BHTV records obtained in the upper part of the hole? Casey et al. (1981) note that some of the thicker flows in the Bay of Islands ophiolite complex show co-

lumbar, polygonal jointing. We see no regular subvertical structures in the massive flows found in the shallow sections of the hole.

An alternative explanation would be that a subvertical hole drilled in a field of thin, subvertical dikes would intersect dike margins every 50–100 m or so. Thus, the observed periodicity of fracture zones could be a result of the hole encountering chill zones every 50–100 m. However, this is not a valid explanation as it is possible to discern steeply dipping dike contacts in the BHTV records obtained in the bottom of Hole 504B. They have a different character and orientation from the features discussed in this section (see Appendix A).

The plots in Figures 11A–C indicate that the pattern of fracturing varies systematically down the hole. That is, zones of intense fracturing occur every 50 m or so

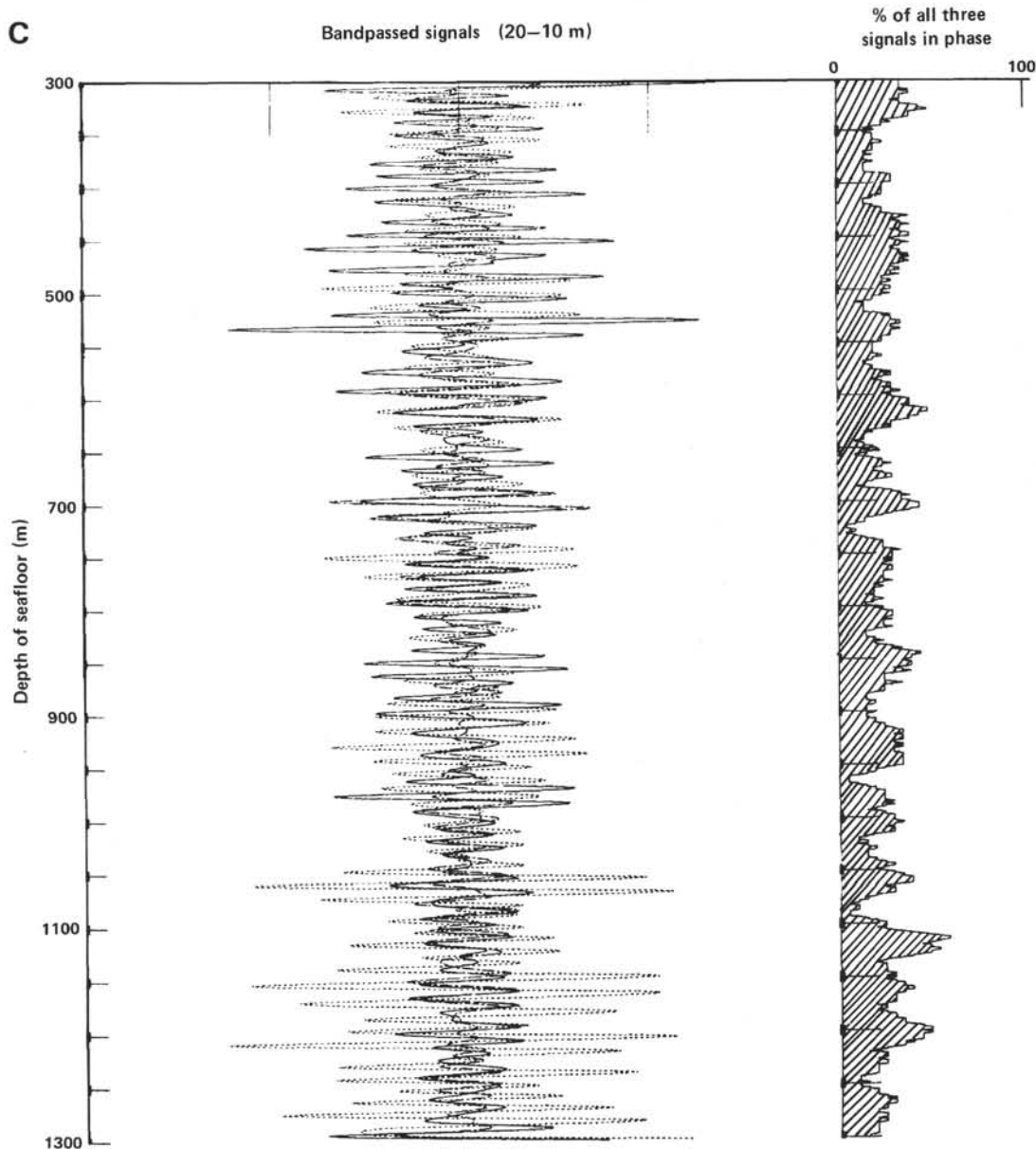


Figure 11. (Continued).

down the hole, separated by less highly fractured intervals. Speculations regarding the manner in which these structures originate can be found in Appendix C.

CONCLUSIONS

Correlation of the downhole geophysical logs and recovered cores from Hole 504B has given us insight into the cause of some of the geophysical changes in the upper layers of the oceanic crust.

Ultrasonic BHTV logging reveals detailed *in situ* structures not apparent otherwise, because core recovery was low during drilling in the hole.

Physical characteristics of the oceanic crustal Layers 2A, 2B, and 2C, such as the detailed sonic velocity structure and changes in the lithostratigraphic structure with depth, are revealed through analysis and cross-correlation of the sonic, BHTV, and electrical resistivity logs.

Analysis and cross-correlation of the sonic, BHTV, electrical resistivity, and nuclear logs reveal a first-order picture of not only the extent but the nature of porosity in the crustal Layers 2A, 2B, and 2C in Hole 504B.

A schematic view of our present understanding follows.

Layer 2A is composed of mostly thin flow units and pillows. The average pillow diameter and flow thickness decreases with depth, although large-diameter pillows and thicker flow units are not uncommon. Porosity is in the form of large, open cracks and drained pillows.

Layer 2B is composed mainly of thin flows and small-diameter pillows. It is a site of intense fracturing, alteration, and pervasive plugging of cracks by secondary mineralization. Zones of brecciation are common. Its porosity can be considered to be of a vesicular character.

Layer 2C is composed mainly of massive, "welded" units, although a few pillows appear above 4520 m (1046.5 m BSF). Although altered, it contains a much smaller bulk content of hydrated minerals and has some open cracks. It is generally less fractured (on a large scale) than the overlying section.

Detailed analysis of the logging data indicates that there is some fundamental pattern of structure in the oceanic crust. The predominant orientation of macrofractures indicates a stress regime in which the minimum stress is vertical at the time of fracturing.

Lastly, it is important to note that these results are based on data from *one hole* in the oceanic crust. Many of the features discussed in this paper may be peculiar to this location and not representative of oceanic crust everywhere. Lacking similar data from other holes, one cannot interpret these phenomena to be characteristics of "typical" crust. We feel that it is imperative that this type of dedicated experimentation be performed in holes drilled in oceanic crust of varying ages in order to learn how the oceanic crust evolves through time.

ACKNOWLEDGMENTS

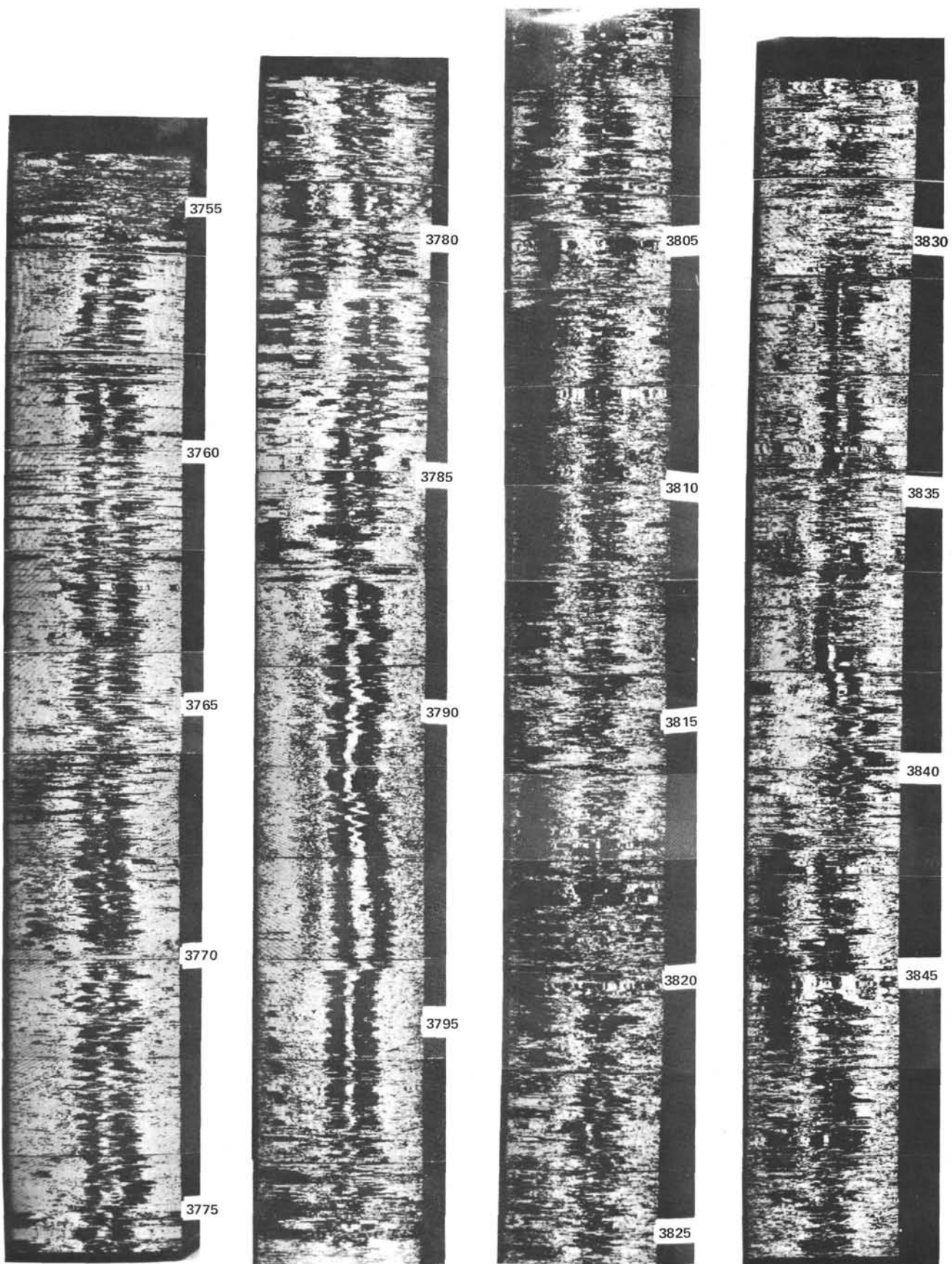
We thank the officers, crew, and scientific party of *Glomar Challenger*, Leg 83, without whose hard work and diligence these logs could not have been successfully completed. Bill Menke provided valuable computer assistance. Terry Engelder, Daniel Fornari, and three anonymous reviewers greatly improved the content of this. This work was supported by Office of Naval Research Contract TO-0098, Scope HH, and National Science Foundation Grants OCE-78-27026 and OCE-81-10919. Contribution 3612 of the Lamont-Doherty Geological Observatory of Columbia University.

REFERENCES

- Anderson, R. N., Honnorez, J., Becker, K., Adamson, A. C., Alt, J. C., Emmermann, R., Kempton, P. D., Kinoshita, H., Laverne, C., Mottl, M. J., and Newmark, R. L., 1982. DSDP Hole 504B, the first reference section over 1 km through Layer 2 of the oceanic crust. *Nature*, 300:589-594.
- Anderson, R. N., and Zoback, M. D., 1982. Permeability, underpressures and convection in the oceanic crust near the Costa Rica Rift, eastern equatorial Pacific. *J. Geophys. Res.*, 87:2860-2868.
- Balk, R., 1937. *Structural behavior of igneous rocks*. Geol. Soc. Am. Mem. 5.
- Becker, K., Langseth, M.G., Von Herzen, R.P., and Anderson, R.N., 1983. Deep crustal geothermal measurements, Hole 504B, Costa Rica Rift. *J. Geophys. Res.*, 88:3447-3457.
- Becker, K., Von Herzen, R.P., Francis, T.J.G., Anderson, R.N., Honnorez, J., Adamson, A. C., Alt, J. C., Emmermann, R., Kempton, P.D., Kinoshita, H., Laverne, C., Mottl, M.J., and Newmark, R. L., 1982. *In situ* electrical resistivity and bulk porosity of the oceanic crust Costa Rica Rift. *Nature*, 300:594-598.
- Cann, J. R., Langseth, M. G., Honnorez, J., Von Herzen, R. P., White, S.M., et al., 1983. *Init. Repts. DSDP*, 69: Washington (U.S. Govt. Printing Office).
- Casey, J. F., Dewey, J. F., Fox, P.J., Karson, J.A., and Rosencrantz, E., 1981. Heterogeneous nature of oceanic crust and upper mantle: a perspective from the Bay of Islands ophiolite complex. In Emiliani, C. Ed.), *The Sea* (Vol. 7), *The Oceanic Lithosphere*: New York (John Wiley and Sons, Inc.), pp. 305-338.
- CRRUST, 1982. Geothermal regimes of the Costa Rica Rift, east Pacific, investigated by drilling, DSDP-IPOD Legs 68, 69, and 70. *Geol. Soc. Am. Bull.*, 93:862-875.
- Decker, R. W., Einarsson, P., and Mohr, P. A., 1971. Rifting in Iceland: new geodetic data. *Science*, 173:530-533.
- Delaney, P. T., 1982. Rapid intrusion of magma into wet rock: ground water flow due to pore pressure increases. *J. Geophys. Res.*, 87: 7739-7756.
- Dietz, R. S., 1963. Alpine serpentinites as oceanic rind fragments. *Geol. Soc. Am. Bull.*, 74:947-952.
- Fox, P.J., Schreiber, E., and Peterson, J.J., 1973. The geology of the oceanic crust: compressional wave velocities of oceanic rocks. *J. Geophys. Res.*, 78:5155-5172.
- Fox, P.J., and Stroup, J. B., 1981. The plutonic foundation of the oceanic crust. In Emiliani, C. (Ed.). *The Sea*, (Vol. 7), *The Oceanic Lithosphere*: New York (John Wiley and Sons, Inc.), pp. 199-218.
- Helmberger, D. V., and Morris, G. B., 1970. A travel time and amplitude interpretation of marine refraction profile: transformed shear waves. *Seismol. Soc. Am. Bull.*, 60:593-600.
- Hess, H.H., 1962. History of ocean basins. In *Petrologic Studies — A Volume in Honor of A. F. Buddington*: New York *Geol. Soc. Am.*, pp. 599-620.
- Hickman, S. H., Langseth, M. G., and Svitek, J. F., 1984. *In situ* permeability and pore pressure measurements near the Mid-Atlantic Ridge, Deep Sea Drilling Project Site 395. In Hyndman, R. D., Salisbury, M. H., et al., *Init. Repts. DSDP*, 78B: Washington (U.S. Govt. Printing Office), 699-708.
- Houtz, R., and Ewing, J., 1976. Upper crustal structure as a function of plate age. *J. Geophys. Res.*, 81:2490-2498.
- Hyndman, R. D., 1979. Poisson's ratio in the oceanic crust — a review. *Tectonophysics*, 59:321-333.
- Hyndman, R. D., and Drury, M. J., 1976. The physical properties of oceanic basement rocks from deep sea drilling on the Mid-Atlantic Ridge. *J. Geophys. Res.*, 81:4042-4059.
- Lachenbruch, A. H., 1961. Depth and spacing of tension cracks. *J. Geophys. Res.*, 66:4273-4292.
- O'Connell, R. J., and Budiansky, B., 1974. Seismic velocities in dry and saturated cracked solids. *J. Geophys. Res.*, 79:5412-5426.
- Orcutt, J. A., Kennett, B.L.N., and Dorman, L.M., 1976. Structure of the East Pacific Rise from an ocean bottom seismometer survey. *Geophys. J. R. Astron. Soc. (WEST)*, 45:305-320.
- Rosencrantz, E., 1983. The structure of sheeted dikes and associated rocks in North Arm Massif, Bay of Islands Ophiolite Complex, and the intrusive process at mid-ocean spreading centers. *Can. J. Earth Sci.*, 20:787-801.
- Schreiber, E., and Fox, P.J., 1976. Compressional wave velocities and mineralogy of fresh basalts from the FAMOUS area and the Oceanographer Fracture Zone and the texture of Layer 2A of the oceanic crust. *J. Geophys. Res.*, 81:4071-4076.
- Schreiber, E., and Fox, P.J., 1977. Density and P-wave velocity of rocks from the FAMOUS region and their implication to the structure of the oceanic crust. *Geol. Soc. Am. Bull.*, 88:600-608.
- Seeburger, D. A., and Zoback, M.D., 1982. The distribution of natural fractures and joints at depth in crystalline rock. *J. Geophys. Res.*, 87:5517-5534.
- Sigurdsson, O., 1980. Surface deformation of the Krafla fissure swarm in two rifting events. *J. Geophys.*, 47:154-159.
- Spudich, P., and Orcutt, J., 1980. A new look at the seismic velocity structure of the oceanic crust. *Rev. Geophys. Space Phys.*, 18: 627-645.
- Stephen, R. A., 1983. The oblique seismic experiment on Deep Sea Drilling Project Leg 70. In Honnorez, J., Von Herzen, R.P., et al., *Init. Repts. DSDP*, (69): Washington (U.S. Govt. Printing Office), 301-308.
- Stephen, R. A., and Harding, A. J., 1983. Travel time analysis of borehole seismic data. *J. Geophys. Res.*, 88:8289-8298.
- Zemanek, J., Glen, E. E., Jr., Norton, L. J., and Cardwell, R. L., 1970. Formation evaluation of inspection with the borehole televiewer. *Geophysics*, 35:254-269.
- Zoback, M. D., and Anderson, R. N., 1982. Ultrasonic borehole televiewer investigation of oceanic crustal layer 2A, Costa Rica Rift. *Nature*, 295:393-397.

Date of Initial Receipt: 18 April 1983

Date of Acceptance: 14 January 1984



Appendix A. Figure 1. Borehole televiewer logs, Hole 504B. Depth below rig floor, in m. For a discussion, see p. 509.

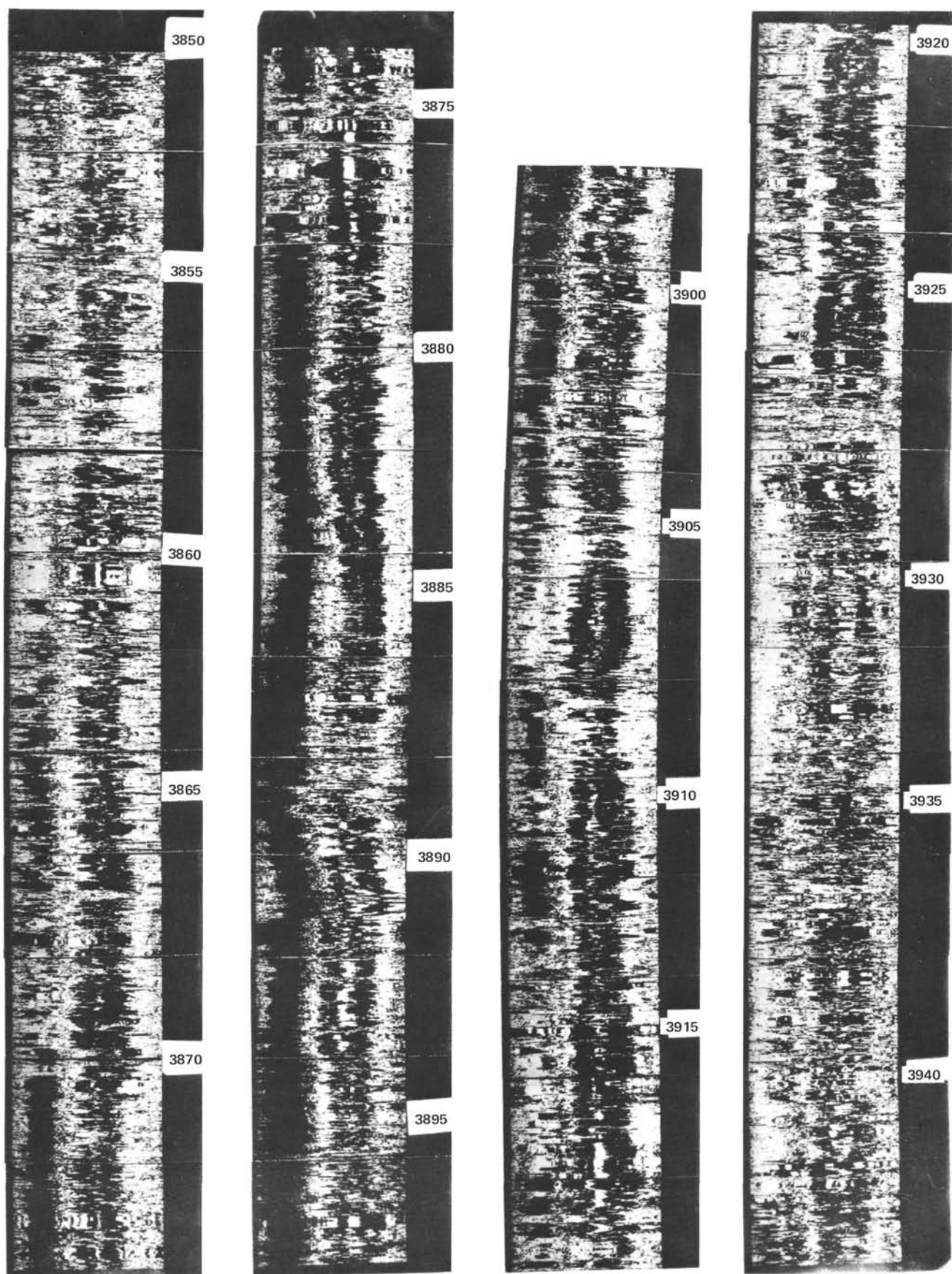


Figure 1. (Continued).

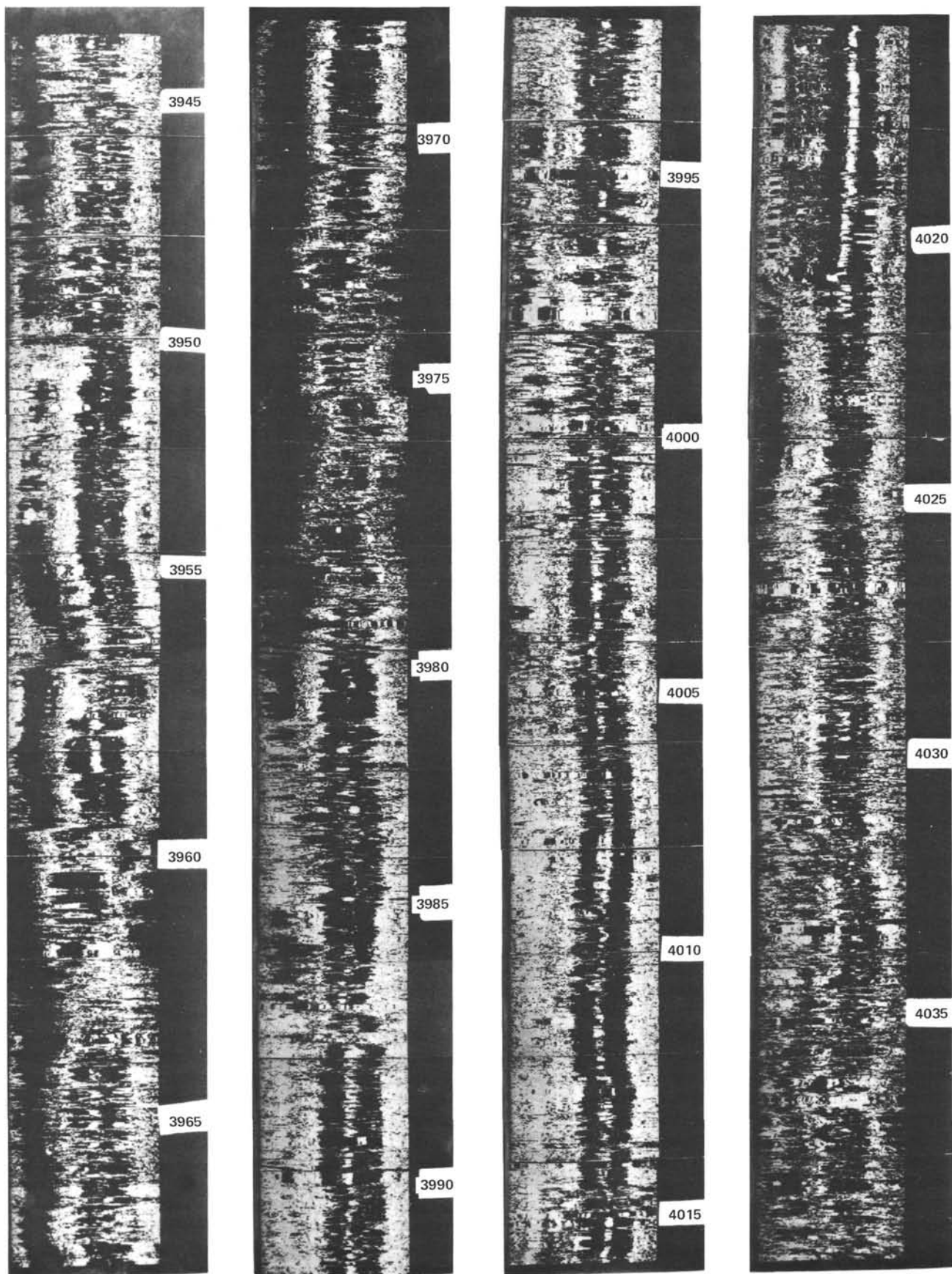


Figure 1. (Continued).

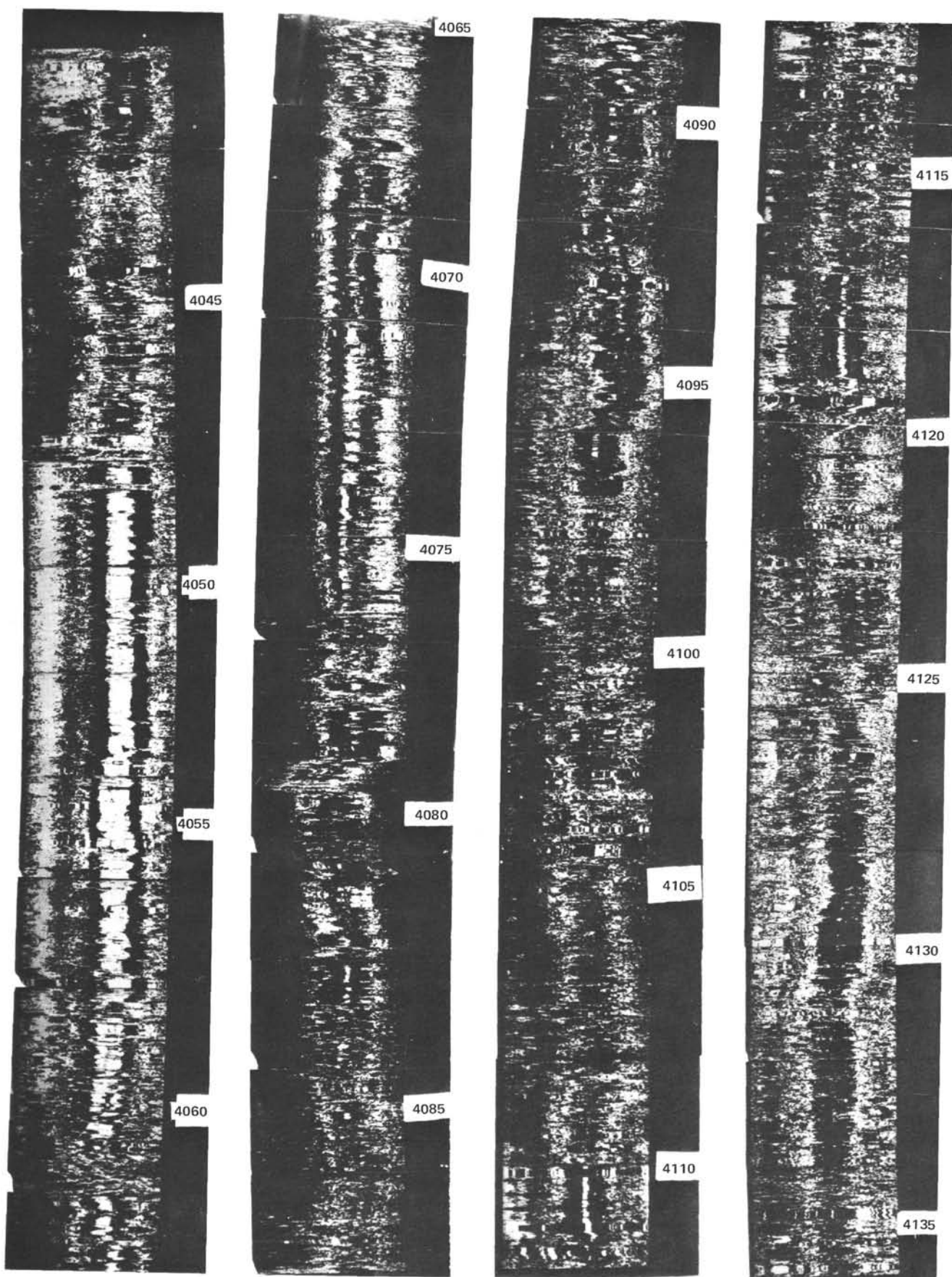


Figure 1. (Continued).

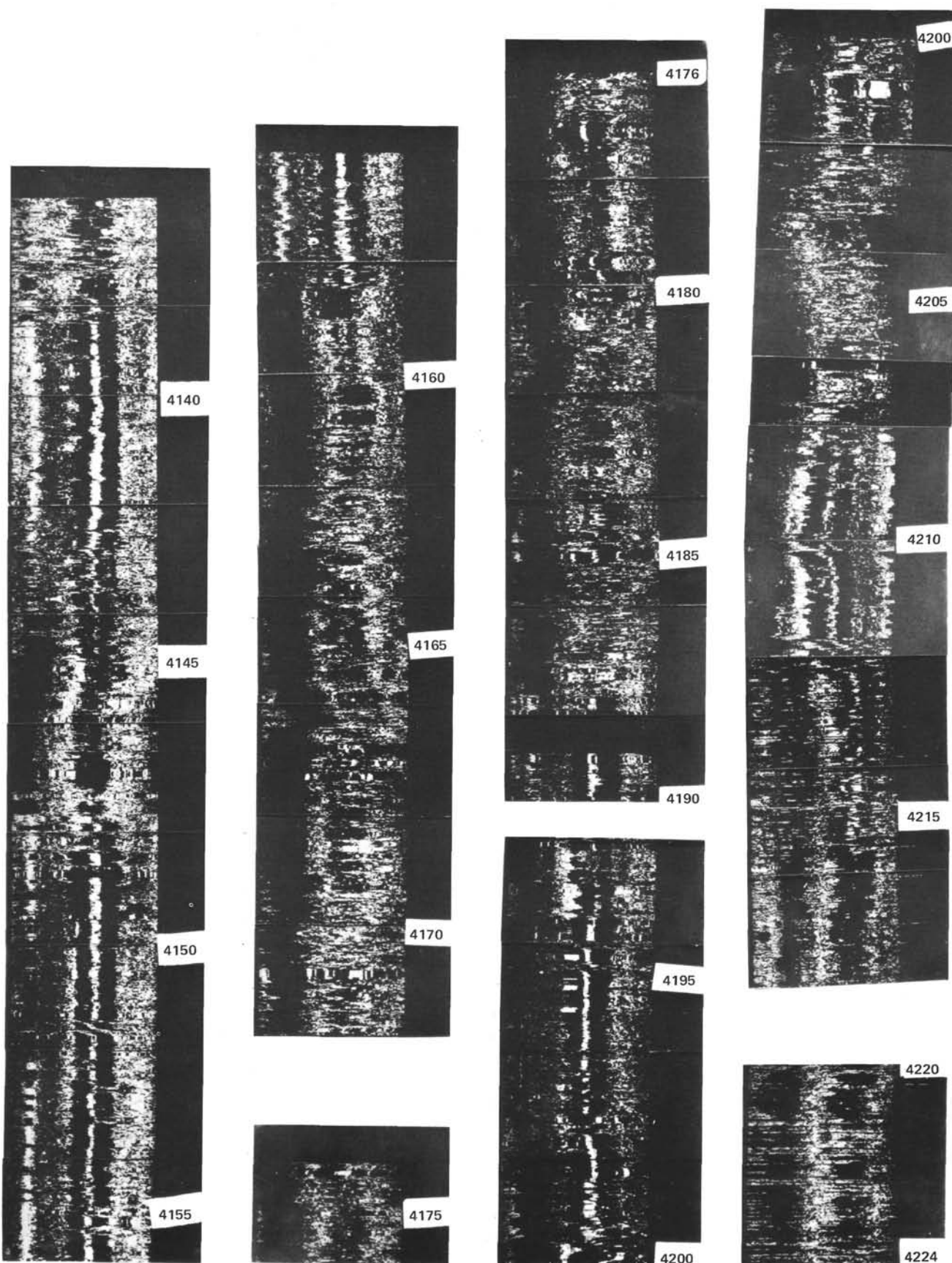


Figure 1. (Continued).

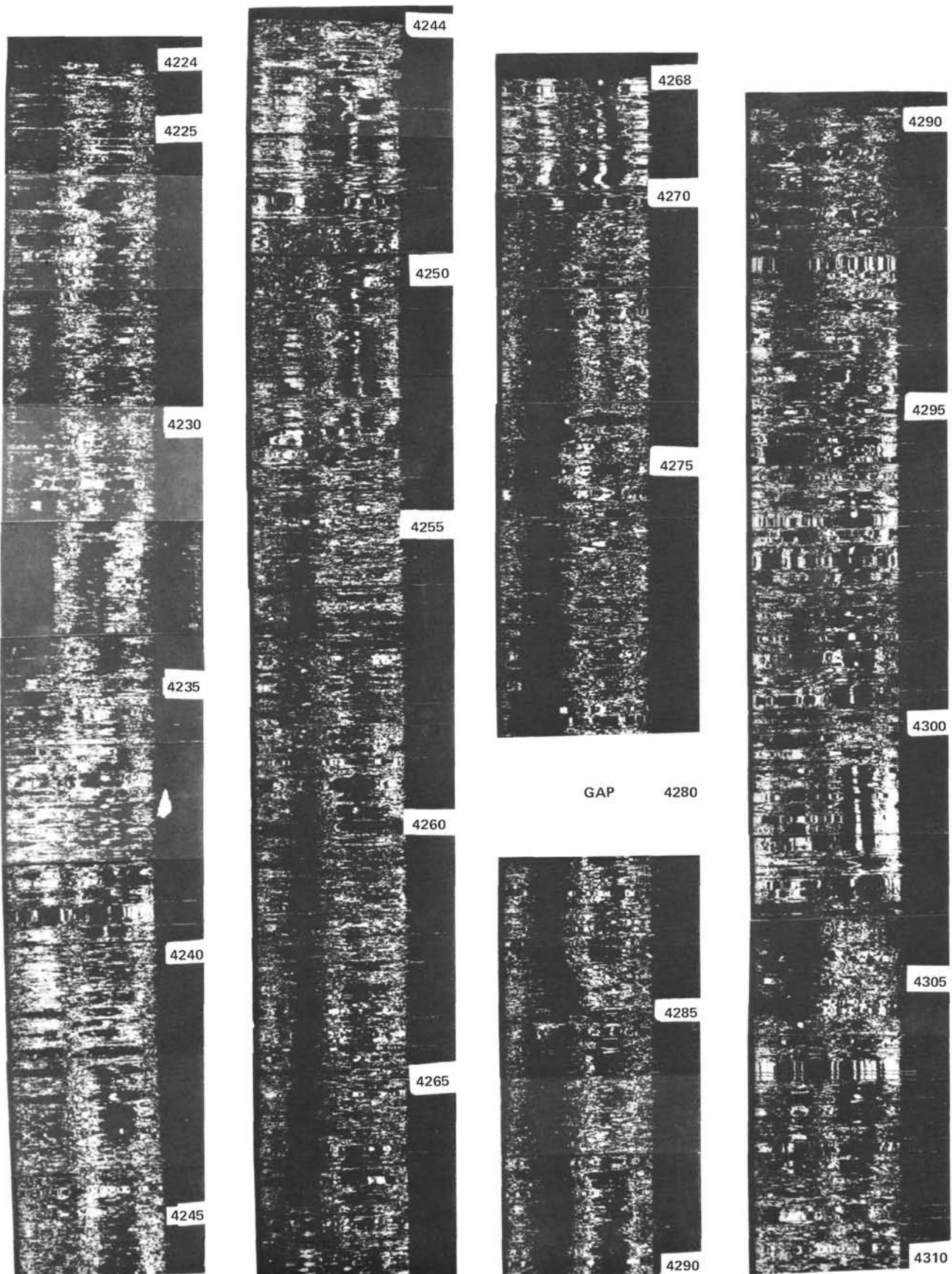


Figure 1. (Continued).

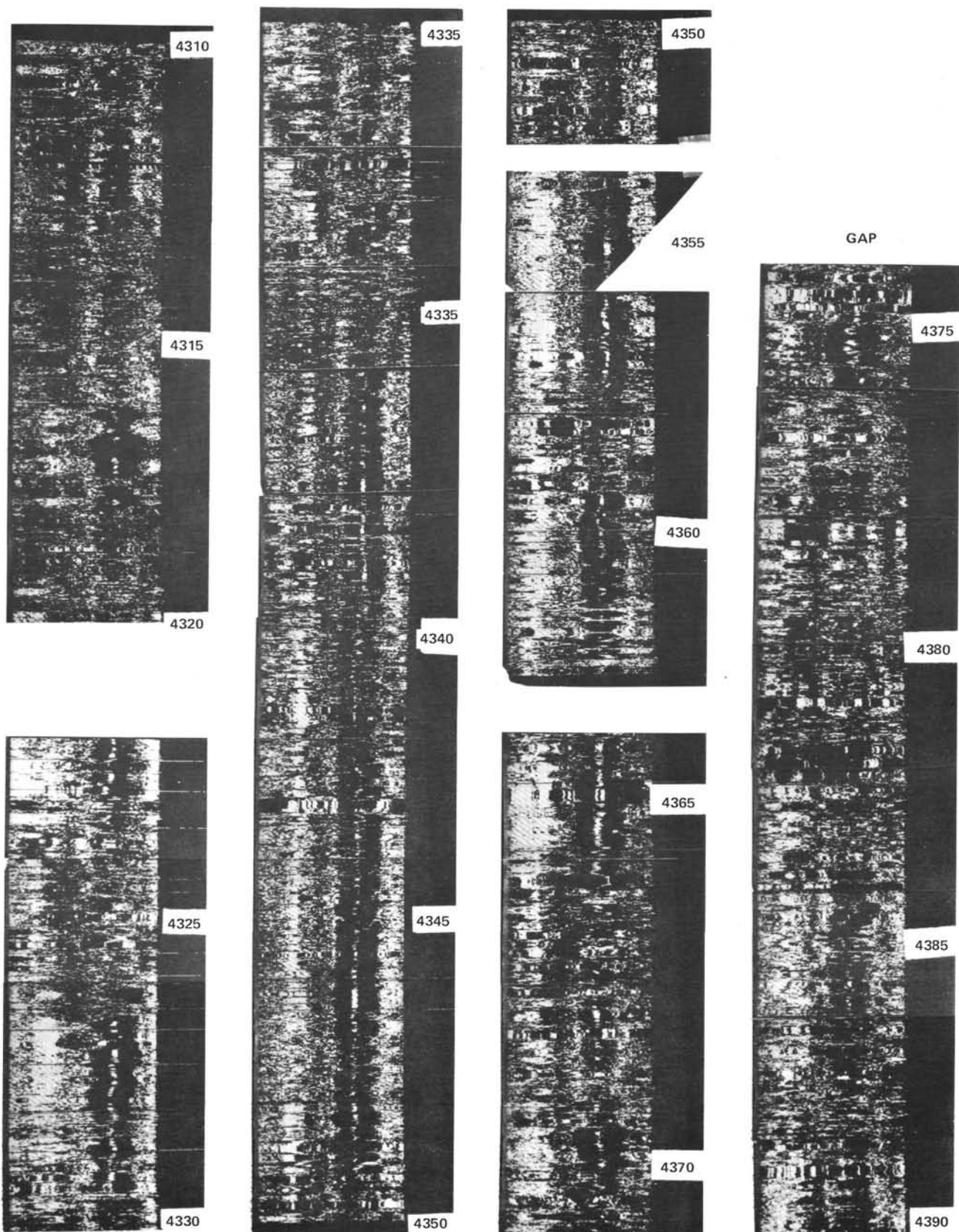


Figure 1. (Continued).

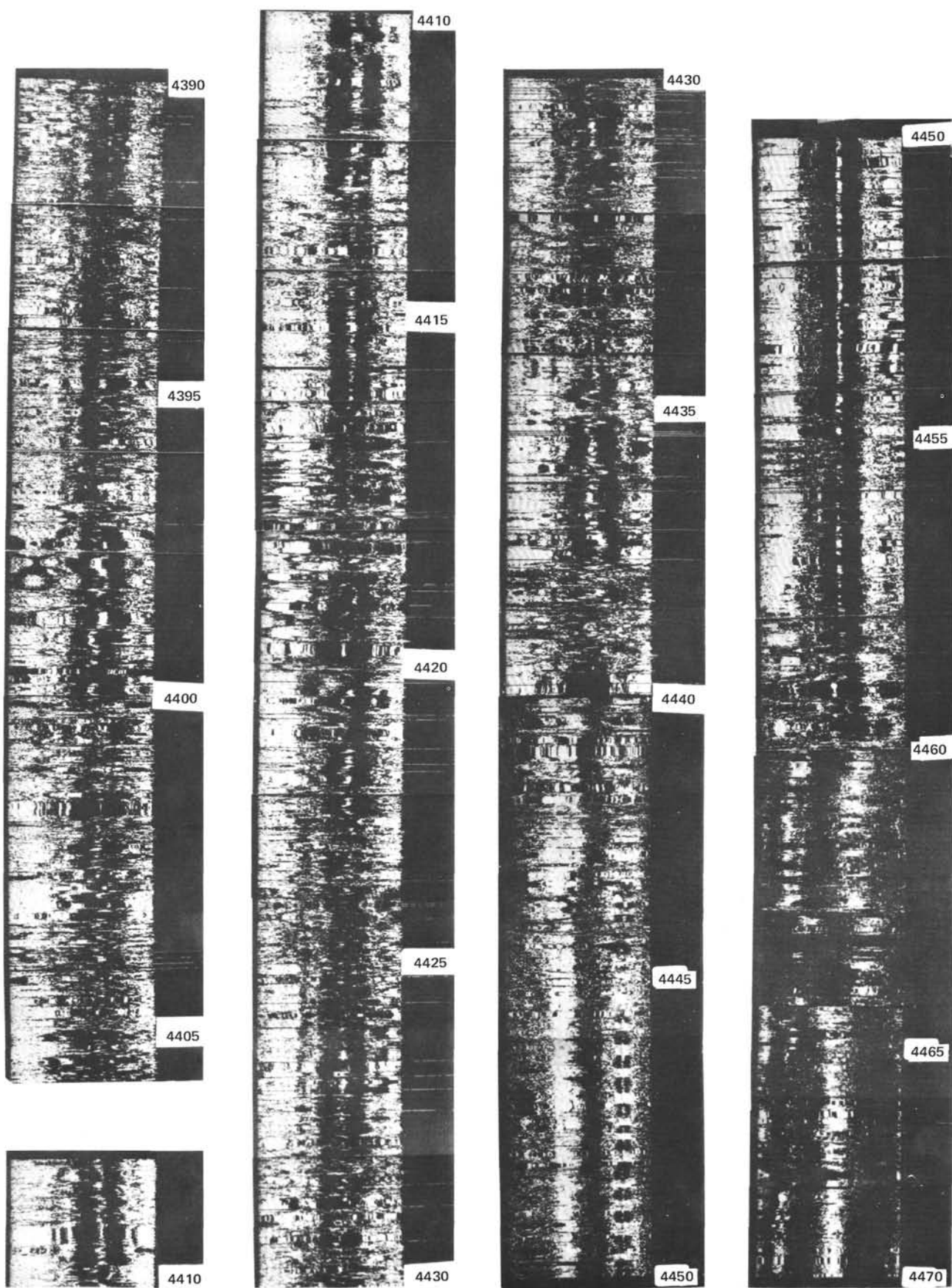


Figure 1. (Continued).

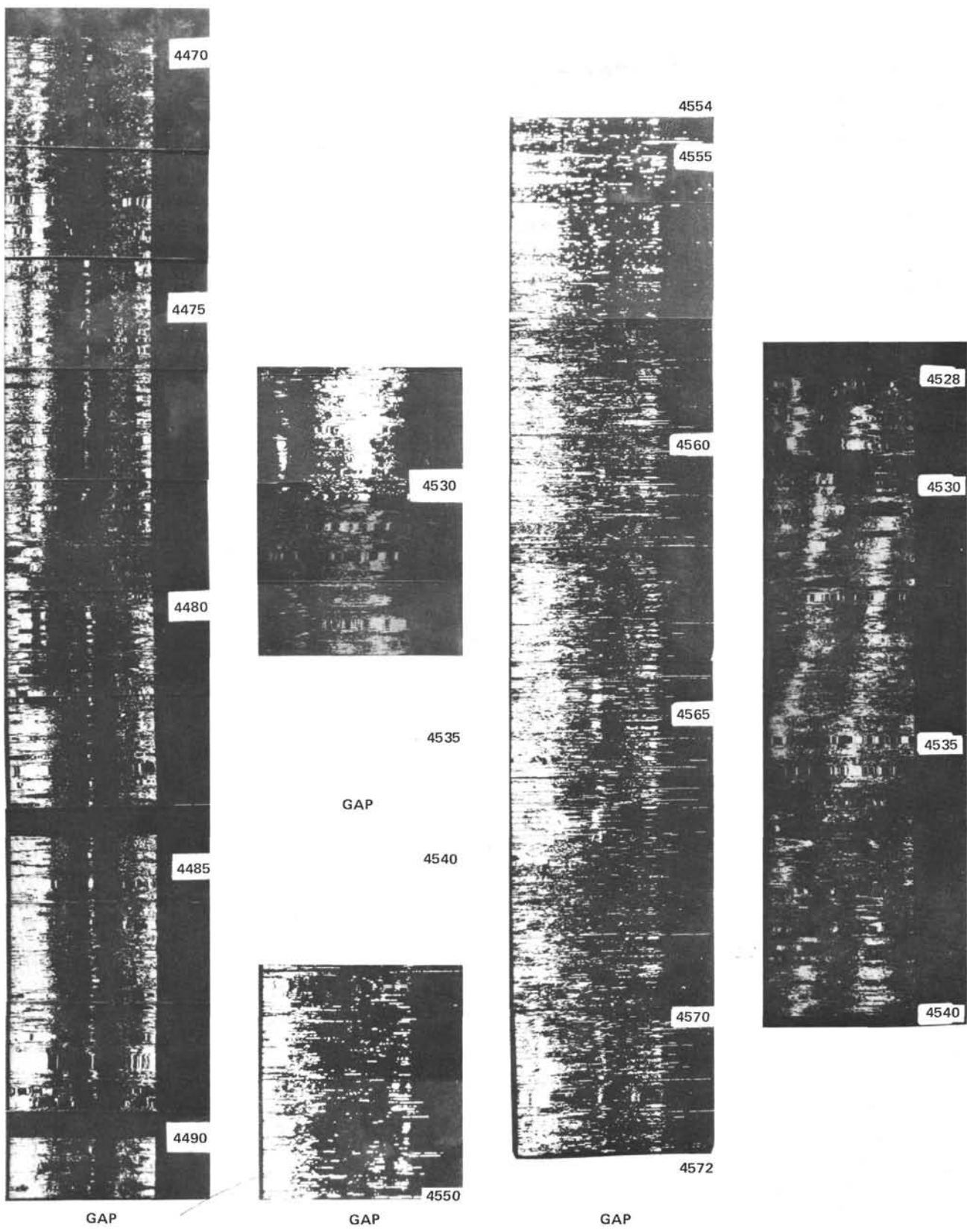


Figure 1. (Continued).

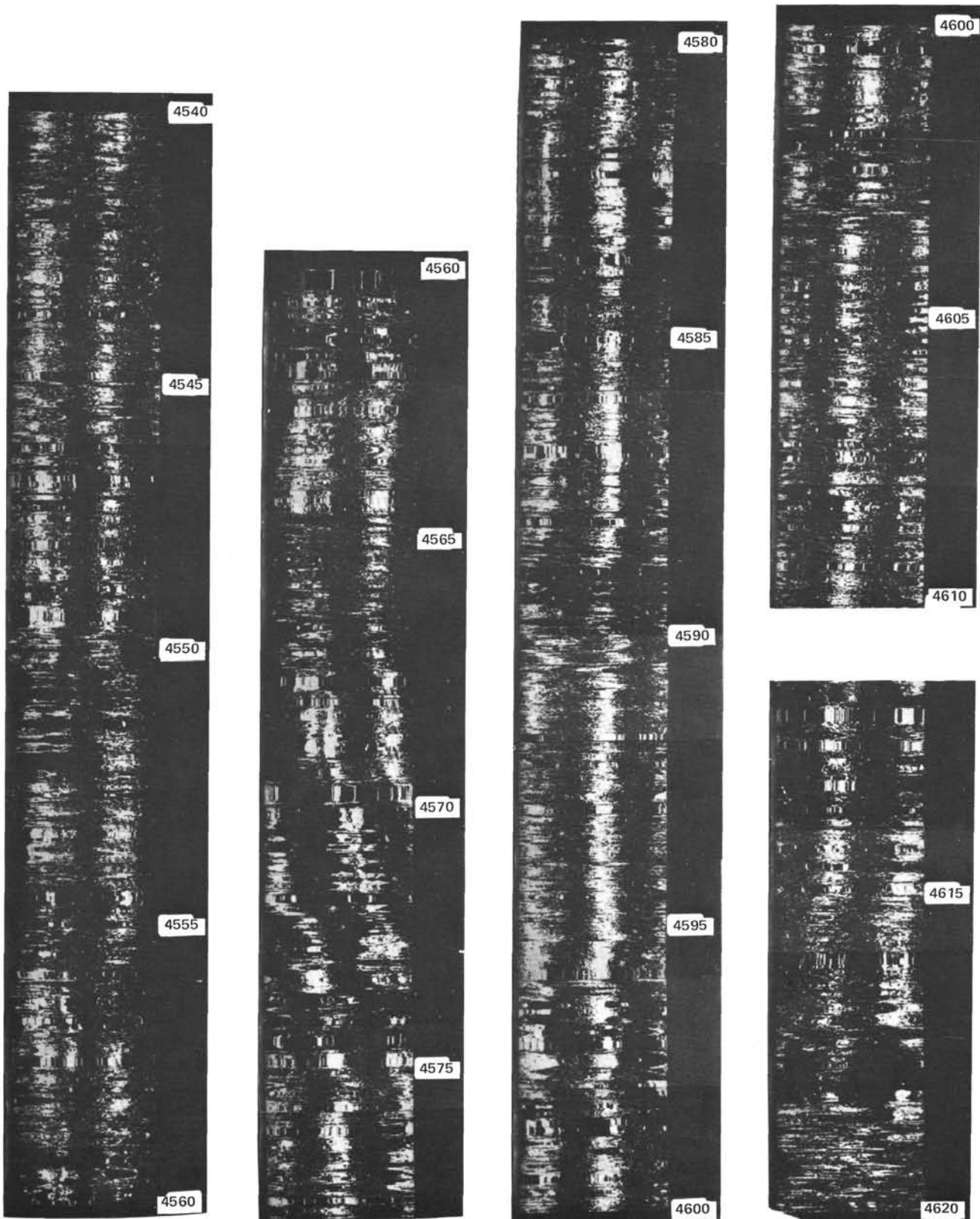


Figure 1. (Continued).

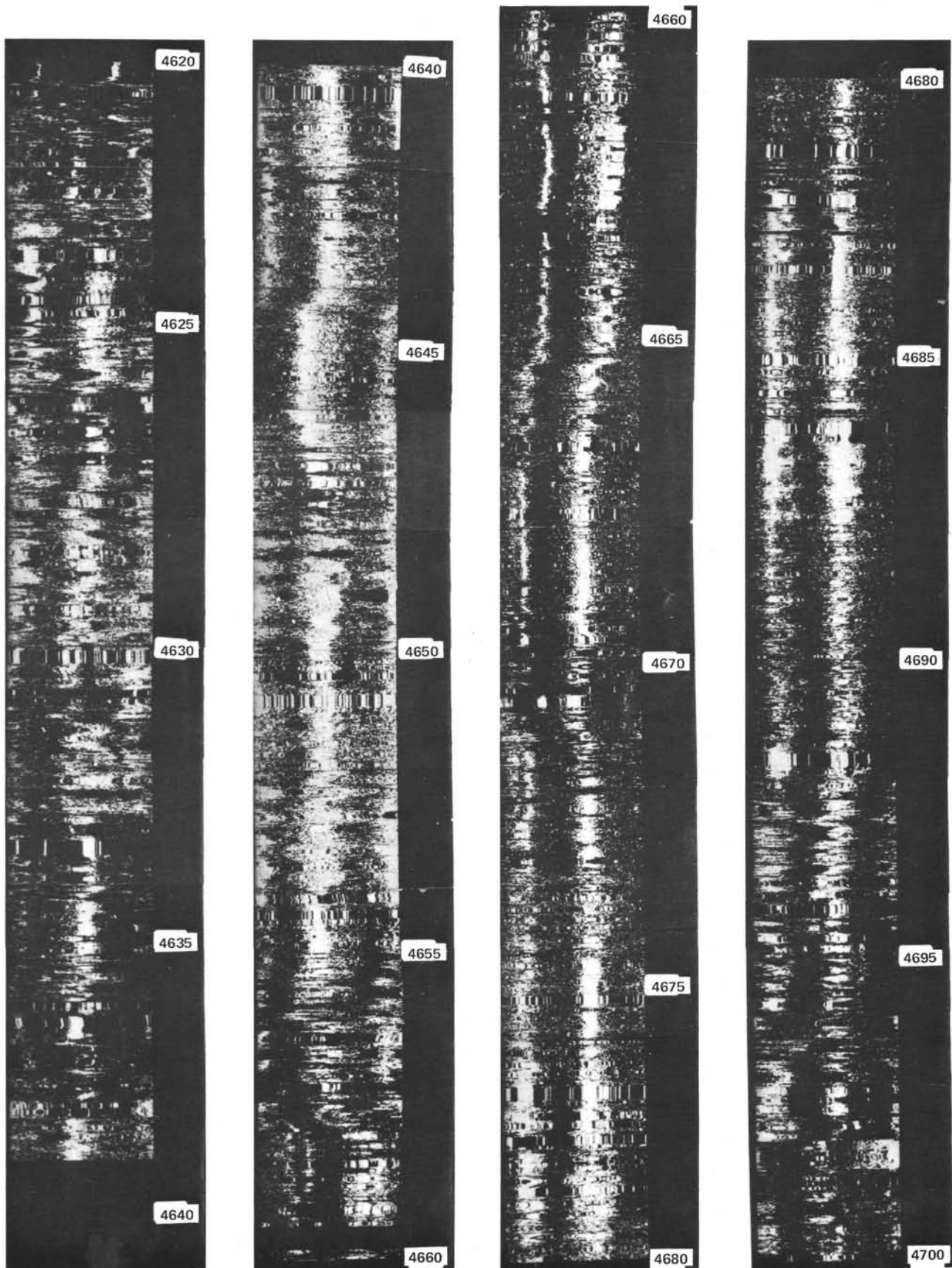


Figure 1. (Continued).

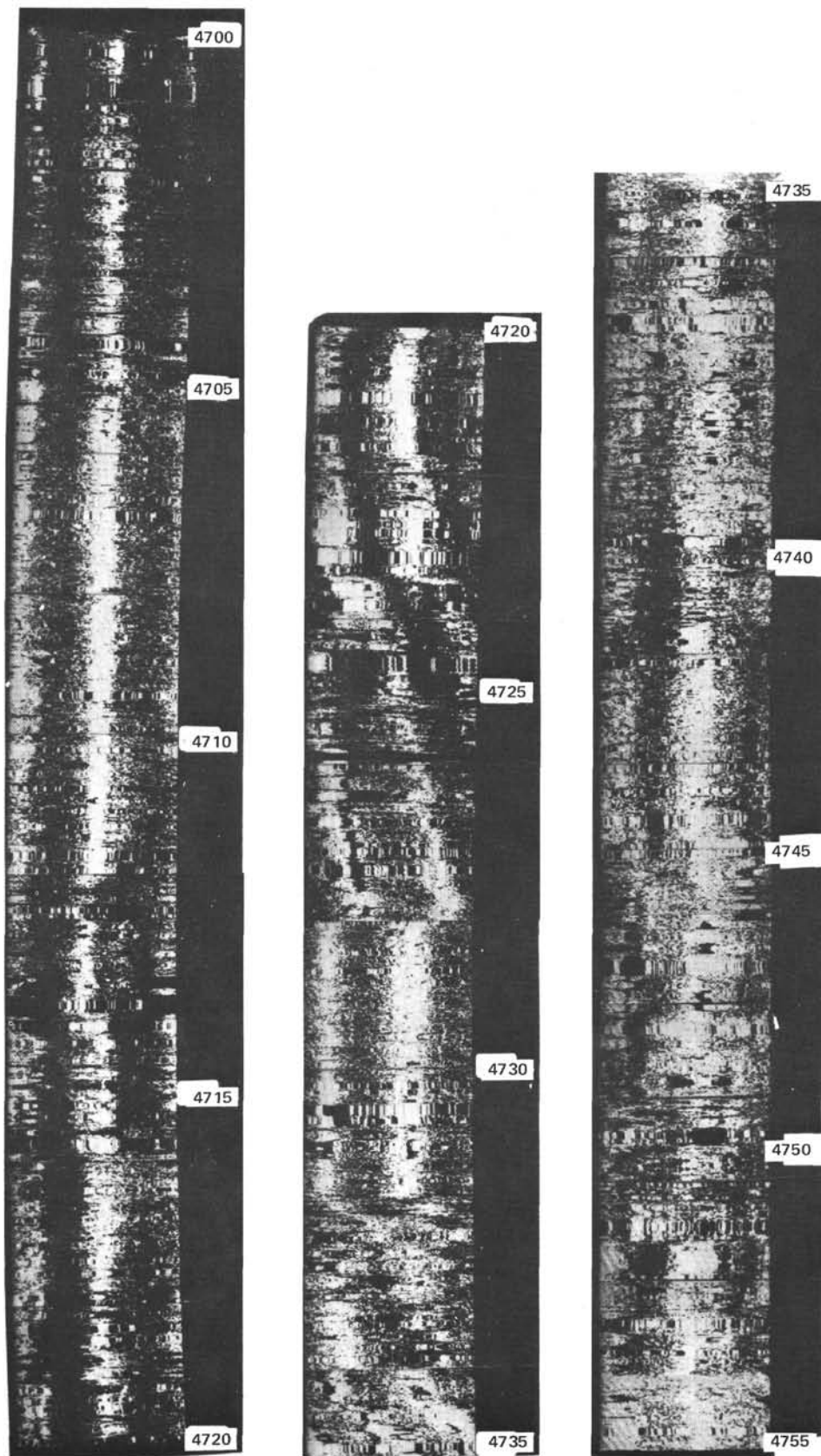


Figure 1. (Continued).

APPENDIX A

Borehole Televiewer Records and Stratigraphic Structure of Hole 504B

In the borehole televiewer records obtained in DSDP Hole 504B (Appendix A, Fig. 1) there is a 2-m offset difference between depths given in the Leg 69 BHTV logging run and the Leg 83 logs, which causes the Leg 83 logs to read about 2 m deeper. All depths given are in meters below the rig floor, which is 3743.5 m above the seafloor.

The upper 50 m of basalt at Hole 504B is composed mostly of thick flow units, with numerous horizontal to subhorizontal fractures such as those seen at 3760–3762 and at 3766 m (286.5–288.5 and 292.5 m BSF respectively). There are several thin interbeds of large-diameter (~30 cm) pillow units, such as at 3762, 3763, 3767, 3768, 3775–3780, and 3784 m (288.5, 289.5, 293.5, 294.5, 301.5–306.5, and 310.5 m BSF respectively). A 10-m-thick massive flow can be seen from 3787 to 3797 m (313.5–323.5 m BSF). From 3806 to 3825 m (332.5–351.5 m BSF) there is an anomalous low-reflectance zone, where structure can be seen although the reflectance amplitude is much lower than in the surrounding zones. Numerous thin flows (<1 m) and pillows occur in the interval from 3825 to 3950 m (351.5–476.5 m BSF). The average pillow diameter decreases from ~20–30 to generally <10 cm, although larger pillows are not uncommon. The average flow thickness decreases from nearly 1 m to more commonly 10–30 cm. Fracturing is predominantly horizontal to subhorizontal and tends to concentrate at the borders of and parallel to separate flow units, as can be seen near 3916, 3919, and 3935 m (442.5, 445.5, and 461.5 m BSF, respectively). This may be analogous to flow-parallel fracturing as seen in ophiolites (Rosencrantz, 1983; Balk, 1937) where fractures are associated with flow top margins. Steeply dipping or vertical fractures are rarely seen in the BHTV record.

From 3950 to 4400 m (476.5–926.5 m BSF), the appearance of the record is darker, indicating a generally lower level of reflectance, which is a characteristic of the records through Layer 2B. There are several zones that are quite dark, such as 3970–3980, 4060–4085, and 4158–4185 m (496.5–506.5, 586.5–611.5, and 684.5–711.5 m BSF, respectively). In some cases this is a result of the hole being washed out or “broken out” so that the diameter is locally enlarged. For example, between 3970 and 3980 m (496.5 and 506.5 m BSF), the caliper shows a significant increase in hole diameter. This generally dark character is more likely caused by the softer nature of the rock, the result of increased clay alteration as observed in the recovered cores (Alt et al., this volume). There are two large, massive units at 4005–4015, 4048–4058 m (531.5–541.5 and 574.5–584.5 m BSF, respectively), and a few smaller ones such as at 4138–4142 m (664.5–668.5 m BSF). In general, however, this section appears to be composed mainly of thin flows (<20 cm) and small diameter pillows (<10 cm). Fracturing is pervasive, often producing brecciated zones such as those at 4061, 4249, and 4335 m (587.5, 775.5, and 861.5 m BSF, respectively). The most common texture in the records over this part of the hole is dark and mottled.

Below 4400 m (926.5 m BSF) the records appear to be lighter, which is indicative of more solid rock and is a general characteristic of the records through Layer 2C. From 4400 to 4460 m (926.5–986.5 m BSF), the records are fairly light colored and the basalt generally massive looking. This light, solid appearance of the records through Layer 2C is a rather abrupt change from the dark, mottled appearance of the records in the overlying Layer 2B. Individual pillows, some quite large in diameter (to 50 cm), can be seen, for example, in the interval 4416–4420 m (942.5–946.5 m BSF). Chatter marks running down the hole from 4444 to 4450 m (970.5–976.5 m BSF) are probably an artifact of the drilling process. The level of fracturing that is still predominantly horizontal to subhorizontal is diminished from that of the overlying interval. There are no dark zones or areas of washout such as those seen in the overlying section.

Below 4460 m (986.5 m BSF), the level of reflectance drops a bit overall and gradually increases to the bottom of the hole. From 4460 to 4640 m (986.5–1166.5 m BSF) individual flows can sometimes be identified. Fracturing remains quite high and is still predominantly horizontal to subhorizontal. There are some small zones of intense fracturing at 4550 and 4565 m (1076.5 and 1091.5 m BSF). Below 4640 m (1166.5 m BSF), the records are of a lighter color and have a gener-

ally solid appearance. Individual units are difficult to identify, whereas there are long zones of solid, regular texture from 4648–4654, 4705–4712, and 4728–4730 m (1174.5–1180.5, 1231.5–1238.5, and 1254.5–1256.5 m BSF, respectively). The level of fracturing decreases. There are two thick (~50 cm) steeply dipping features at 4732–4734 and 4750–4754 m (1258.5–1260.5 and 1276.5–1280.5 m BSF, respectively). Because of the diffuse nature and steep inclination of these features, they have been interpreted as dike contacts. The overall massive or solid appearance of this lowermost section of the hole as seen in the BHTV images agrees well with descriptions of the sheeted dike unit of the Bay of Islands ophiolite as being “massive coherent rock composed of separate but tightly welded dikes” (Casey et al., 1981; Rosencrantz, 1983).

APPENDIX B

Derivation of Phase Difference, $D(\omega)$ ¹

We can describe two log signals F_1 and F_2 as time series where the “frequency” is 1/wavelength along the hole, or depth, with amplitudes $A_1(\omega)$, $A_2(\omega)$ and phases φ_1 and φ_2 :

$$\begin{aligned} F_1 &= A_1(\omega) e^{i\varphi_1} \\ F_2 &= A_2(\omega) e^{i\varphi_2} \end{aligned}$$

We normalize the amplitudes and thus the phase difference, $D(\omega)$, is

$$\begin{aligned} \frac{1}{4} \left| \frac{F_1(\omega)}{A_1(\omega)} + \frac{F_2(\omega)}{A_2(\omega)} \right|^2 &= \frac{1}{4} |e^{i(\varphi_1)} + e^{i(\varphi_2)}|^2 \\ &= \frac{1}{4} \left\{ 2[1 + \cos(\varphi_1 - \varphi_2)] \right\}^2 \\ &= \frac{1 + \cos(\varphi_1 - \varphi_2)}{2} \\ &= 1 \text{ when } \varphi_1 = \varphi_2 \\ &= 0 \text{ when } \varphi_1 = -\varphi_2 \end{aligned}$$

Appendix B, Figure 1 shows phase difference, $D(\omega)$, plotted versus phase offset in degrees.

¹ This analysis was designed by William Menke in February 1982, at Lamont-Doherty Geological Observatory, Palisades, N.Y.

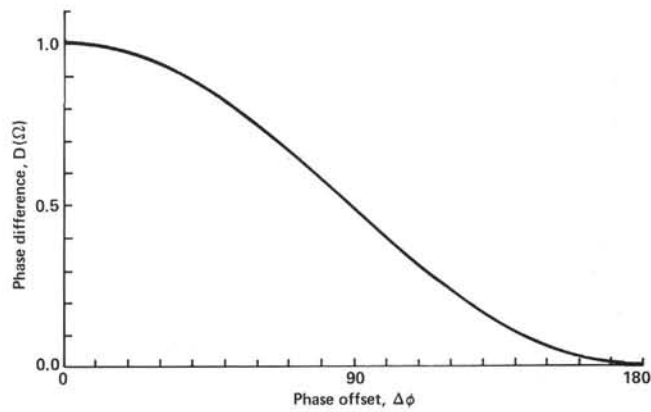


Figure 1. Phase difference, $D(\omega)$, plotted versus phase offset in degrees. Since this function depends on the cosine of the phase difference, signals completely in phase will yield a value of 0.0, signals 180° out of phase will yield a value of 0.85, and completely random signals will yield an average value of 0.5.

APPENDIX C
Possible Origins of Fracturing in Hole 504B

Because the fracturing appears to be mainly subhorizontal, the minimum horizontal stress must have been greater than the vertical stress at the time of fracturing (if no major preexisting fractures were present in the formation). In other words, the minimum horizontal stress must have been greater than the lithostatic, or over 200 bars (see, also, Hickman et al., 1984; Anderson and Zoback, 1982; and CRRUST, 1981).

Delaney (1982) has presented a theoretical analysis that can be used to describe the local pressure increase due to the heating of ground water in wet rock upon injection of hot magma. He addresses the short-term heat transfer problem, when thermal pressurization is dominant and before buoyant flow is set up. His formulation indicates that in some cases pressure increases may be great enough to cause natural hydraulic fracturing of the host rock.

If we apply values of bulk permeability, porosity, and compressibility from Hole 504B to his model we obtain the interesting result that the pressure increase resulting from the injection of a dike into the rocks of the lower section of Hole 504B might be on the order of 300–500 bars, which could cause natural hydraulic fracturing of the host rock. These cracks would then be horizontal, because the horizontal stresses would be greater than the vertical stress ($S_H > S_V$). This is a possible mechanism by which many of the shallow-dipping fractures in the lower part of the hole could originate.

Of course, there is no way of being certain that the permeability and porosity structure present in Hole 504B now is representative of the conditions present 6 m.y. ago when this crust was being formed. However, we do not believe the dike rocks were dry when they were situated at the ridge axis. Alt et al. (this volume) has described three stages of alteration present in the rocks recovered from Hole 504B. The first is a high-temperature alteration that most likely occurred when the site was located on the ridge axis. The second is a low-temperature alteration that occurred when the site was located off-axis. The last is a high-temperature phase resulting from the high-temperature regime the site is subjected to at present (Alt, this volume). The early high-temperature phase and the stockwork that was formed when the site was located at the ridge axis attest to the extensive hydrothermal activity occurring at or shortly after the time of dike intrusion. The shallow dikes reached to or near the seafloor itself. After a short time, the dike section was progressively buried by pillows and flows. Under these conditions, the shallower parts of the very young dike section might encounter seawater flowing through the basaltic pillow carapace at the same time they were being intruded by new dikes. Given these conditions, thermal pressurization might cause natural hydraulic fracturing in the shallow dike section.

If this were the cause of the observed structure at Hole 504B, then the spacing of the fractures with depth might indicate the depth of thermal relief for each intrusive pulse. In addition, one would expect the spacing of the fractures to increase with depth until they were no longer found. The observation that the fracture spacing increases through layers 2B and 2C seems to support this idea.

Another possible mechanism by which these structures originate would be mechanical rebound. It is known that a form of mechanical rebound occurs in rift zones after rifting and intrusion (Decker et al., 1971; Sigurdsson, 1980). Appendix C Figure 1 shows data from Krafla, Iceland (Sigurdsson, 1980). The top curve shows the elevation change from leveling lines over a rift zone immediately post-rift. Below this are plotted the triangulation data over the same region. As expected, horizontal extension occurred over the area of the rift. However, immediately bordering the region of horizontal extension are areas of net horizontal contraction. These zones bordering the rift area went from a regime of net extension to net contraction at the moment of

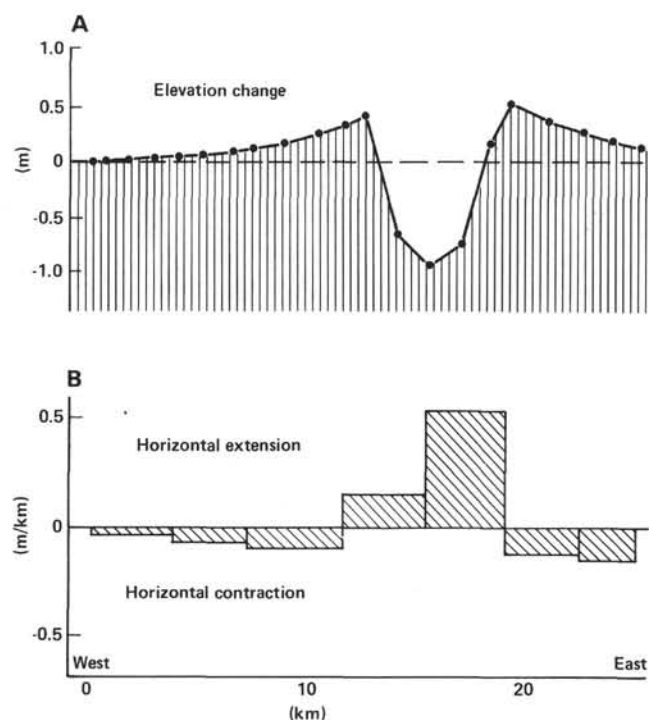


Figure 1. Changes in (A) elevation and (B) horizontal distance associated with the eighth tectonic event during the period December 1975 to May 1979 in Krafla, Iceland (from Sigurdsson, 1980).

rifting, leaving zones of contraction and extension adjacent to each other where extension had been dominant immediately before. This is analogous to a rubber band being stretched, then punctured. The zones immediately bordering the puncture area go from a new extension to a net contraction, while the rest of the rubber band remains in extension.

It is possible that tension relief at the spreading axis because of the intrusion of a dike might cause a similar mechanical rebound. As the dike propagates up through a section of rock that is in an extensional stress regime, tension is relieved almost instantaneously, causing a contraction or rebound in the host rock immediately bordering the new dike. On land there is usually a surficial expression of this rebound (e.g., Decker et al., 1971; Sigurdsson, 1980). There is a surficial downdrop across the rift itself and an uplift immediately bordering the rift zone. The mechanical rebound due to the abrupt change in the local stress regime due to the intrusion of a dike may cause brittle failure in the dikes immediately bordering each newly intruded dike.

If this were the mechanism by which the fracture spacing in Hole 504B originated, the spacing of the fractures with depth is closely related to the episodicity of dike intrusions at the ridge axis, or the rate at which the magma rises to the surface. The amount of porosity in the bordering dikes would influence the process. More fractures would then be predicted in the shallow parts of the dike section than in the deeper ones that should have lower porosity. This agrees with the observation of increased fracture spacing with depth through Layers 2B and 2C.